1 **Influence of bank slope on sinuosity-driven hyporheic exchange flow and**

2 **residence time distribution during a dynamic flood event**

4 Yiming Li[1,2], Uwe Schneidewind[2], Zhang Wen[1*], Stefan Krause[2], Hui Liu[1]

6 [1]Hubei Key Laboratory of Yangtze River Catchment Environmental Aquatic Science,

7 School of Environmental Studies, China University of Geosciences, People's Republic

8 of China

9 [2]School of Geography, Earth and Environmental Sciences, University of Birmingham,

10 UK

12 ***Correspondence:** Zhang Wen (wenz@cug.edu.cn)

Abstract. This study uses a reduced-order two-dimensional (2-D) horizontal model to investigate the influence of riverbank slope on the sinuosity-driven hyporheic exchange process along sloping alluvial riverbanks during a transient flood event. The Deformed Geometry Method (DGM) is applied to quantify the displacement of the sediment-water interface (SWI) along the sloping riverbank during river stage fluctuation. This new modeling approach serves as the initial step focusing on the impact of bank slope on the hyporheic exchange flux (HEF) and the residence time distribution (RTD) of pore water in the fluvial aquifer for a sinuosity-driven river corridor. Several controlling factors, including sinuosity, alluvial valley slope, river flow advective forcing and duration of flow are incorporated into the model to investigate the effects of bank slope on aquifers of variable hydraulic transmissivity. Compared to simulations of a vertical riverbank, sloping riverbanks were found to increase the HEF. For sloping riverbanks, the hyporheic zone (HZ) encompasses a larger area and penetrated deeper into the alluvial aquifer, especially in aquifers with smaller transmissivity (i.e., due to increased hydraulic conductivity or reduced specific yield). Furthermore, consideration of sloping banks as compared to a vertical river bank can lead to both underestimation or overestimation of the pore water travel time. The impact of bank slope on residence time was more pronounced during a flood event for high transmissivity aquifer conditions, while it had a long-lasting influence after the flood event in lower transmissivity aquifers. Consequently, the impact of bank slope decreases the travel time of water discharging into the river relative to base flow conditions. These findings highlight the need for (re)consideration of the importance of complex riverbank morphology conceptualization in numerical models when account for the HEF and RTD. The results have potential implications for river management and restoration and the management of river and groundwater pollution.

Key words: hyporheic exchange, sloping riverbank, deformed geometry, numerical simulation, residence time distribution

Nomenclature

ΔL	Nodal spacing [m]
$\bigtriangledown$	Laplace operator
α_L	Longitudinal dispersivity [L]
α_T	Transverse dispersivity [L]
D	Dispersion-diffusion tensor [$L^2 T^{-1}$]
D_L	Water diffusivity [$L^2 T^{-1}$]
J_x	Base groundwater gradient [-]
K	Hydraulic conductivity [LT^{-1}]
n	Scaling number [-]
n_0	Intensity of flood event [-]
n_d	Skewness of flood event [-]
S_y	Specific yield [-]
t_d	Duration of flood event [T]
t_p	Time to peak river stage [T]
α	Amplitude of the river boundary [L]
Γ_d	Dimensionless aquifer transmissivity [-]
δ	Bank slope angle [°]
δ_{ij}	Kronecker delta function [-]
ϵ	Tortuosity [-]
η	Degree of flood event asymmetry [T^{-1}]
θ	Effective porosity [-]
λ	River boundary wave length [L]
σ	River boundary sinuosity [-]
τ	Residence time [T]
ω	Flood event frequency [T^{-1}]
$h(\mathbf{x}, t)$	Transient groundwater head [L]
Δh^*	Dimensionless parameter of ambient groundwater flow [-]

$A^{**}(t)$	Dimensionless variation of HZ area relative to base flow conditions [-]
$C(\mathbf{x}, t)$	Solute concentration in the aquifer [ML^{-3}]
$C_0(\mathbf{x})$	Solute concentration as initial condition [ML^{-3}]
$C_S(\mathbf{x}, t)$	Solute concentration in the river [ML^{-3}]
$d^{**}(t)$	Dimensionless variation of HZ penetration distance relative to base flow conditions [-]
$H(\mathbf{x}, t)$	Thickness of the saturated aquifer [L]
$H_0(\mathbf{x})$	Initial river stage [L]
H_p	Peak river stage during the flood event [L]
$H_r(t)$	River stage at the downstream end [L]
$h_r(x, t)$	Transient river stage [L]
$M(t)$	Displacement of the sediment-water interface [L]
P_e	Péclet number [-]
$\mathbf{q}$	Specific discharge or Darcy flux [LT^{-1}]
$\mathbf{Q}$	Aquifer-integrated discharge [L^{2}T^{-1}]
$Q^*_{in, HZ}(t)$	Dimensionless net flux along the river boundary [-]
$Q^*_{in, HZ}(t)$	Dimensionless exchange flux from the aquifer to the river [-]
$Q^*_{out, HZ}(t)$	Dimensionless exchange flux from the river to the aquifer [-]
$Y(x, t)$	Location of the sediment-water interface boundary [L]
$z_b(\mathbf{x})$	Elevation of the underlying impermeable layer [L]
Γ_d	Dimensionless parameter of aquifer transmissivity [-]
$\mu_r(\mathbf{x}, 0)$	Mean (first order of) residence time distribution [T]
$\mu^*_{out}(x, t)$	Flux-weighted ratio of mean RT to mean RT under baseflow conditions [-]
$\mu_n(\mathbf{x}, t)$	n-th moment of residence time distribution [T^n]
$\mu_r^*(\mathbf{x}, t)$	Mean residence time distribution ratio between slope and vertical river bank model [-]
$\mu_{\tau0\text{-max}}$	Maximum RT in the domain [T]

$\mu_{\tau\text{-}S}(\mathbf{x}, t)$	Mean residence time distribution of slope river bank model [T]
$\mu_{\tau\text{-}V}(\mathbf{x}, 0)$	Mean residence time distribution of vertical river bank model [T]
$\rho(\mathbf{x}, t, \tau)$	Residence time distribution [T]
Abbreviations	
HZ	Hyporheic zone
HEF	Hyporheic exchange flux
DGM	Deformed Geometry Method
SWI	Sediment-water interface
RTD	Residence time distribution
RT	Residence time
ALE	Arbitrary Lagrangian–Eulerian
2-D	Two-dimensional
BTS	Biogeochemical timescale

1. Introduction

44   The hyporheic zone (HZ) can be described as the region that connects the river

45   channel and adjacent aquifer, and includes riverbed and riverbanks. Mixing and

46   transport of different water types (groundwater, surface water) and water ages in the

47   HZ driven by hydrodynamic and hydrostatic factors cause spatially and temporally

48   varying exchange of water and biogeochemical species between river channel, riverbed

49   and aquifer (Cardenas, 2009b; Hester and Gooseff, 2010; Krause et al., 2011, 2017,

50   2022; McClain et al., 2013; Boano et al., 2014). The hyporheic exchange flux (HEF)

51   represents the interaction flux between surface water and groundwater in vertical (e.g.,

52   bedform-driven) and horizontal/lateral (e.g., meander-driven) directions, which can add

53   to general regional groundwater exfiltration and infiltration. The distribution of

54   hyporheic flow paths strongly determines the spatial and temporal distribution of

55   hydrogeochemical characteristics of water within the riverbed and the wider river

56   corridor as well as the formation of so-called hot zones and hot moments (Krause et al.,

57   2013, 2017; Cardenas, 2015; Pinay et al., 2015).

58   HEF is controlled by parameters such as stream discharge dynamics, recharge,

59   riverbed and aquifer hydraulic properties, local hydraulic head fluctuations, as well as

60   river geometry and morphology including sinuosity and riverbank slope (Larkin and

61   Sharp, 1992; Gomez-Velez et al., 2012; 2017; Schmadel et al., 2016). For example,

62   Cardenas et al. (2004) demonstrated how riverbed characteristics and especially the

63   heterogeneity of hydraulic conductivity could increase HEF by 17% to 32%. As such,

64   a better estimation of the relative importance of HEF on catchment water fluxes and

65   biogeochemical processes requires a good understanding of its different drivers and

66   controls. This is imperative as the spatiotemporal progression of HEF, the resulting

67   change in HZ (area) and thus also the residence or travel time (RT) of the exchanged

68   water in the HZ have significant impact on flow dynamics and transient storage along

69   the river continuum and in turn control the capacity for contaminant attenuation

70 (Weatherill et al., 2018) and biogeochemical functions of river corridors (Bertrand et

71 al., 2012; Boulton et al., 2010; Brunke and Gonser, 1997).

72   Both lateral exchange between river and its floodplain, as well as bedform-

73 induced vertical exchange at the streambed interface have been found to be crucial with

74 regards to HEF and the biogeochemical transformation potential along the river corridor

75 (Boano et al., 2010, 2014; Gomez-Velez and Harvey, 2014; Gomez-Velez et al., 2015,

76 2017; Kiel and Cardenas, 2014; Stonedahl et al., 2013). By using numerical simulations,

77 considerable progress has been made with regards to our understanding of how river

78 planform geometry (Boano et al., 2006, 2010; Cardenas 2006; 2008; 2009a, 2009b;

79 Stonedahl 2013), dynamic flood events (Gomez-Velez et al., 2012; 2017) and

80 evapotranspiration (Kruegler et al., 2020) control HEF. Focusing on lateral exchange

81 flow processes, Cardenas (2008; 2009a, 2009b) utilized numerical models to

82 investigate HEF and residence time distribution (RTD) for various river channel

83 morphologies and regional groundwater flow conditions. Their simulations indicate

84 that channel morphology, represented by sinuosity, is a dominant factor controlling HEF,

85 the total HZ area, and RTD. In addition, Boano et al. (2010) used a similar modeling

86 framework to study the relationship between RTD and biogeochemical transformation

87 by introducing surface water as a major source of dissolved organic matter that triggers

88 a sequence of redox reactions within the HZ. Reactive transport simulations showed a

89 good relationship between RTD and denitrification reaction potential. Based on these

90 studies, Gomez-Velez et al. (2012) conducted numerical simulations to investigate the

91 impact of aquifer parameters (water table gradient, hydraulic conductivity, dispersivity)

92 and channel sinuosity on HEF and RTD. The authors analyzed the RTD for various

93 aquifer conditions to study when a meander can play a role as both source or sink of

94 nitrate. More recent modeling studies focused predominantly on the effects of dynamic

95 river/groundwater stage fluctuations on lateral (e.g., Schmadel et al., 2016; Gomez-

96 Velez et al., 2017) and vertical (e.g., Singh et al., 2019, 2020; Wu et al., 2018, 2020,

97 2021) hyporheic exchange and RTD. For example, Gomez-Velez et al. (2017) explored

98   the HZ response to a dynamic river stage due to variable hydraulic conductivity,

99   groundwater flow gradient and river sinuosity conditions. Their results indicate that

100   during a flood event the dynamic forcing greatly influences net HEF, the area of the HZ

101   as well as mean RTD across different settings, whereby the aquifer transmissivity is one

102   of the key parameters.

103   Although there is a considerable body of numerical research on the lateral

104   hyporheic response to the various geometrical (e.g., geometry of river channel, river

105   slope, etc) and dynamic drivers (e.g., fluctuation of river/groundwater, gaining and

106   losing stream conditions, etc.), many HZ studies do not specifically consider

107   floodplain-driven processes or they assume vertical riverbanks with straight river

108   planimetry in an attempt to reduce model complexity in line with the analytical or

109   numerical solutions used (Cooper and Rorabaugh, 1963; Hunt, 1990; Schmadel et al.,

110   2016; Gomez-Velez et al., 2017;). However, riverbanks are usually sloping (inclined)

111   rather than vertical (Liang et al., 2018) as they undergo erosion (by surface and

112   subsurface water) and gravity collapse (Osma and Thorne, 1988; Fox and Wilson, 2010).

113   Previous research has proven that bank erosion and bank collapse are controlled by

114   various factors, such as initial bank slope angle (Zingg, 1940; Lindow et al., 2009),

115   surface flow forces (Hagerty et al., 1995; Fox and Wilson, 2010), vegetation cover

116   (Mayor et al., 2008; Gao et al., 2009; Puttock et al., 2013) and sediment properties

117   (Millar and Quich, 1993). Previous studies have demonstrated that neglecting bank

118   slope when modelling riverbank hyporheic exchange may have significant impact on

119   model prediction accuracy (Doble et al. 2012a, 2012b; Liang et al. 2020) and RTD

120   (Derx et al., 2014; Siergieiev et al., 2015) in an unconfined floodplain aquifer. Thus, a

121   detailed analysis of the floodplain drivers of HEF should require a more detailed

122   consideration of the floodplain geometry including riverbank slope in bank storage

123   conceptual models (Sharp, 1977).

124   A few previous studies have used numerical modeling where the model is bounded

125   by a sloping riverbank to assess the influence of bank slope on HEF for a vertical section

of an alluvial aquifer. In such cases, the aquifer was considered variably saturated, homogenous, and isotropic, while flow in the unsaturated zone was calculated using the Richards equation (Li et al., 2008; McCallum et al., 2010; Doble 2012a; b). These studies have confirmed that neglecting bank slope can lead to an underestimation of the bank storage volume as well as the temporal HEF in vertical cross-sectional profiles, especially under relatively small bank angles.

In turn, river sinuosity and ambient groundwater gradient (along the river channel) have not been studied as potential drivers of sinuosity-driven lateral HEF and RTD and their biogeochemical implications when a sloping river bank exists and it needs to be determined whether considering both drivers can lead to significantly different findings as compared to previous cross-sectional profile models (Doble et al., 2012; Siergieiev et al., 2015; Derx et al., 2014). In this study, we therefore quantify the effect of bank slope on the spatial extent (area) of the HZ in sinuosity-driven river meanders in response to a flood event and how it impacts the progression of HEF and RTD under varying aquifer transmissivity conditions to better understand lateral HEF through the alluvial plain. The RTD represents the distribution of average pore water travel time since the infiltration of river water into the system for a given time (Gomez-Velez et al., 2012; Singh et al., 2019). We build on the numerical modeling approach introduced by Gomez-Velez et al. (2017) and consider lateral bank slope by coupling the deformed geometry method (DGM) to the flow (Liang et al. 2020), the solute transport and the residence time distribution equation. Our results reveal how and when bank slope plays an important role in sinuosity-driven meandering rivers with respect to HEF and RTD, which in turn will lead to an improved understanding of the river channel-aquifer-floodplain system and provide guidance on the placement of monitoring locations in river management studies.

2. Methodology

2.1 Model setup using deformed geometry method

The modeling approach and dimensionless parameterization used by Gomez-Velez et al. (2017) can represent most riverbank-aquifer situations and dynamic flood conditions. In our study, we use their conceptual model to set up a baseline case with the same model frame, equations and parameterization metrics. Additional information regarding the implementation of this baseline case can be found in the SI. However, where their previous research assumed a vertical river bank for sinuosity-driven HEF, we consider a sloping riverbank and use the Deformed Geometry Method (DGM) approach to capture the dynamic progression of the surface water interface (SWI) along the river course. A constant sloping angle (δ [°]) along the alluvial riverbank of a sinusoidal river was implemented in our model (see blue lines of conceptual model in Figure S1 and the corresponding mathematical model in Figure S2a) while the SWI was assumed to be always vertical (vertical solid red and green lines in Figure S2c). As such, the contraction or expansion of the simulated domain, i.e., displacement of the SWI can be characterized by the sloping angle (there is no movement of the SWI for the vertical riverbank case) and river stage. As the river stage changes, so does the location of the SWI.

When the river stage changes in our model, the sinusoidal boundary will migrate towards or away from the floodplain meaning that the submerged part of the riverbank is considered contracted and our model only considers the alluvial aquifer that is not submerged. The changes of the SWI during a flood event can be calculated by considering river stage and bank slope via:

$$Y(x, t) = Y_0(x) + M(t) \tag{1}$$

where $Y(x, t)$ [L] is the location of the SWI boundary while $Y_0(x)$ [L] is the initial

177 location of the SWI. $M(t) = [h(t) - h(0)]/\tan(\delta)$ is the displacement of the SWI in y-

178 direction due to river stage fluctuation and bank slope angle (see the horizontal distance

179 between the vertical red and green solid line in Figure S2c). In contrast to the vertical

180 riverbank models of Gomez-Velez et al. (2017), $M(t)$ is added in Eq. (1) to simulate

181 sloping riverbank conditions.

182   To simulate the model domain deformation and mesh displacement, we use the

183 DGM interface in COMSOL Multiphysics (COMSOL) (COMSOL Multiphysics, 2019).

184 In this interface, the deforming feature of a specified domain can be defined as a

185 boundary condition with a given moving velocity or displacement. DGM is based on

186 the arbitrary Lagrangian–Eulerian (ALE) method, which is a hybrid method that allows

187 both the model domain and mesh to move or deform simultaneously in a predefined

188 manner. More details on ALE can be found in Donea et al. (2014). While it has

189 previously been used for simulating general free-surface problems (e.g., Duarte et al.,

190 2004; Maury, 1996; Pohjoranta and Tenno, 2011), to our knowledge, DGM has not yet

191 been implemented to solve moving boundary problems in hyporheic exchange studies.

192 Here we used Eq. (1) as an input to the DGM interface to simulate the displacement of

193 the SWI (water flow) during a dynamic flood event. Infiltration and seepage face before

194 and after the peak time of the flood event, respectively, were neglected (Boano et al.,

195 2006; Cardenas. 2009a, b; Kruegler et al., 2020). Fig. 1 illustrates the river stage

196 hydrograph of this study (Fig. 1a, calculated by Eq. (S2), where $t^* = t/t_d$, t_d is the

197 duration of flood event) and the diagram of the displacement of the SWI (Fig. 1b)

198 during the flood event after coupling DGM into the model. The colored river boundaries

199 in Fig. 1b are corresponding to the times of colored dots in Fig. 1a. Additionally, solute

200 transport and mean RTD were simulated based on the extent of the flow field according

201 to Gomez-Velez et al. (2017), as shown in the SI (S2 and S3, respectively).

202
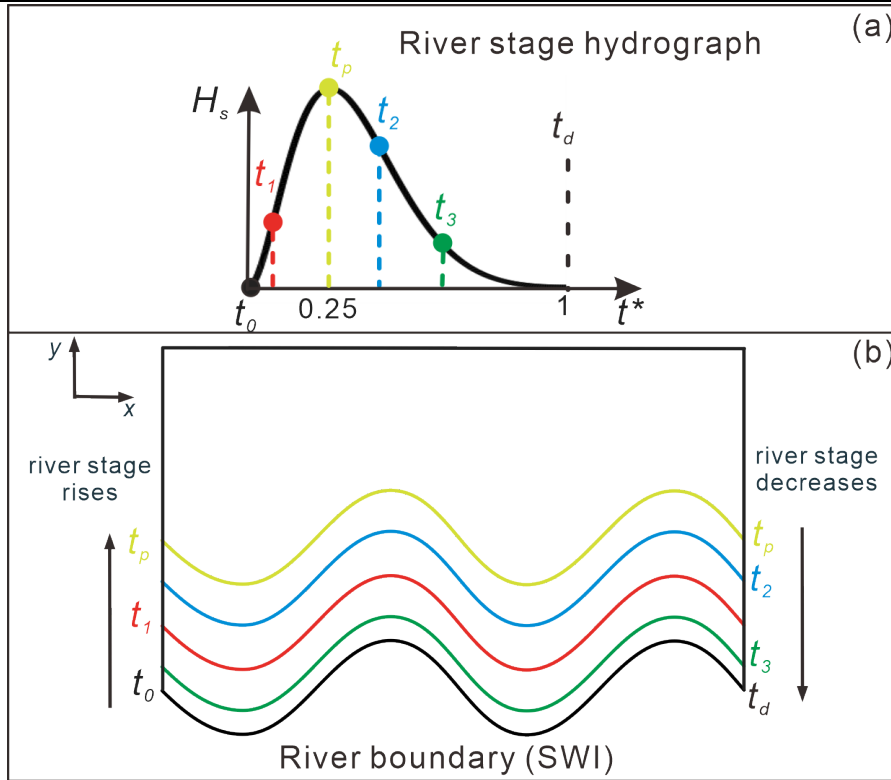
Figure 1. (a) River stage hydrograph during the flood event; (b) diagram showing displacement of SWI during the flood event. The colored SWIs in (b) correspond to the times of colored dots in (a). When the river stage increases, the river boundary migrates into the aquifer and recovers to its initial location as river stage decreases as also indicated by the arrows.

2.2 Model parameterization, testing and scenarios

Hydraulic conditions used in our numerical modeling study are based on values from Gomez-Velez et al. (2017), who conducted a Monte Carlo analysis. They found that the dynamic variations of HEF and mean RTD are mainly determined by ambient groundwater flow and the ratio of aquifer hydraulic conductivity to the duration of the flood event, referred to as dimensionless constant $\Gamma_d = \frac{S_y \lambda^2}{0.5K(1+n_0)H_0 t_d}$, (see Table 1 and Fig. S2), where S_y is specific yield [-]; λ is wave length of sinuous river; K is hydraulic conductivity [LT^{-1}]; n_0 is intensity of the flood event [-] H_0 is base river stage [L]; t_d is duration of the flood event [T]).

After setting up the baseline model case with a vertical riverbank ($\delta = 90°$), we compared our model results for that case with those obtained by Gomez-Velez et al. (2017) for (a) net HEF represented by $Q^*_{net, HZ}(t)$; (b) area of HZ, $A^{**}(t)$; (c) penetration of the HZ, $d^*(t)$ for $\Gamma_d = 0.1$, 1, 10 and 100, and found that our model simulated those cases with high accuracy (Fig. 2). Parameters $A^{**}(t)$ and $d^*(t)$ are based on modeling the transport of a conservative solute while $Q^*_{net, HZ}(t)$ is based on modeling water flow. Slight differences between our model and that of Gomez-Velez et al. (2017) might be due to the use of a much more refined mesh in this study as well as different length scales.
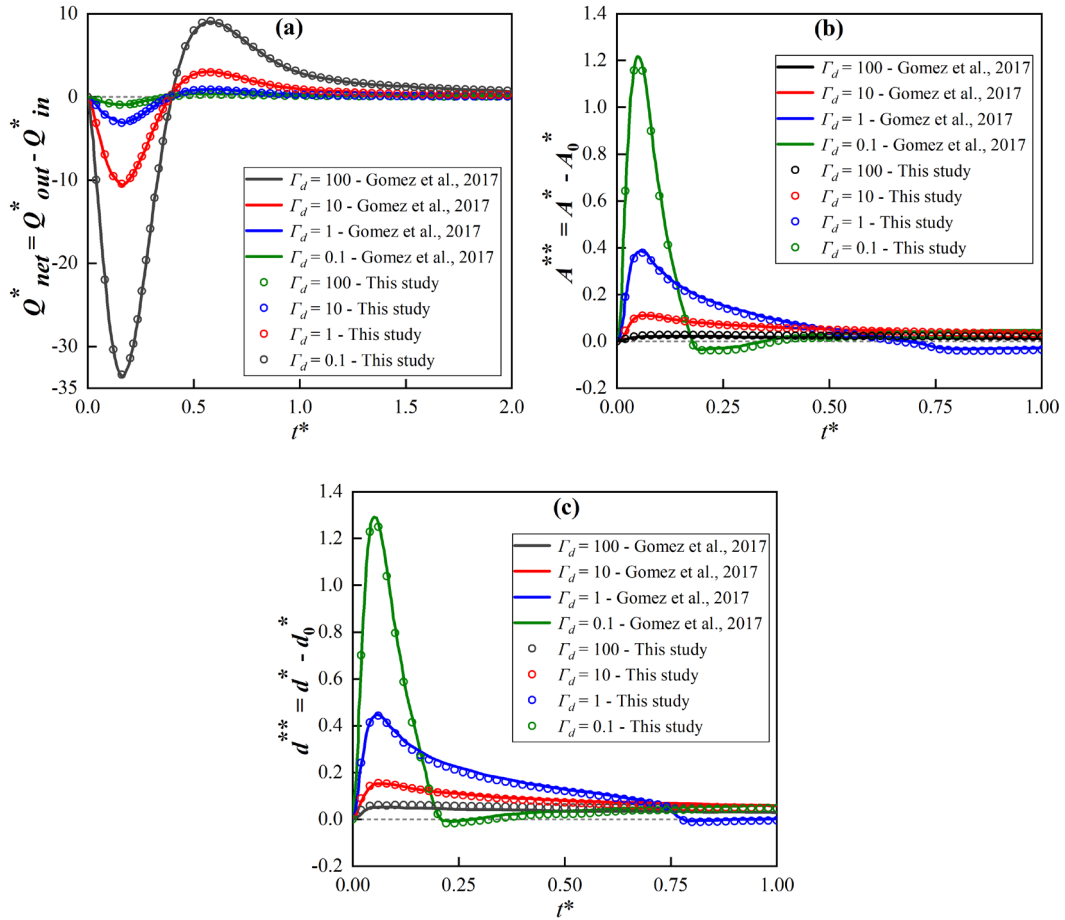
Figure 2. Comparison of results obtained in this study with those of Gomez et al. (2017) for the baseline case with a vertical river bank and variable Γ_d: (a) net hyporheic exchange flux represented by $Q^*_{net, HZ}(t)$; (b) extent of the hyporheic zone $A^{**}(t)$ and (c)

234   penetration distance $d^*(t)$ of the hyporheic zone into the alluvial valley. A more refined

235   mesh and different length scales used in this study can explain slight variations between

236   our model and that of Gomez et al. (2017). Information regarding model fits can be

237   found in the SI.

238   To test, whether our assumption of considering a vertical SWI and using the DGM

239   to characterize the migration of the SWI was appropriate, we compared the vertical 2-

240   D model with a 1-D model coupled with the DGM. Detailed information on this

241   comparison as well as validation results are provided in the SI in section S4. The results

242   show that our approach is reasonable when simulating HEF in a sloping riverbank

243   aquifer.

244   We then considered a series of riverbank scenarios where the bank slope angle

245   was varied, ranging from $\delta = 90°$ (vertical riverbank) to 10° (nearly horizontal case)

246   and Γ_d values ranged from 0.1 to 100, corresponding to aquifer hydraulic conductivity

247   ranging from 480 to 0.048 m/d, indicating high to low transmissivity. Table 1 presents

248   the parameters used in our numerical modeling study. The finite-element models

249   proposed in this study were set up using the COMSOL Multiphysics (COMSOL)

250   software. Eq. (S1), Eq. (S3) and Eq. (S6) were implemented by using a customized

251   Partial Differential Equation (PDE) interface to include the Boussinessq equation,

252   vertical integrated solute transport equation and equation for calculating residence

253   (travel) time distributions (RTD), respectively. The model domain was discretized into

254   about 0.5 million variably-sized triangular elements, with refinement imposed near the

255   river boundary. Mesh-independent numerical solutions are achieved by limiting grid

256   size (ΔL) to less than 0.2 m. Thus, the transverse and longitudinal Peclet numbers

257   (calculated by $P_e = \Delta L/\alpha_L$ and $P_e = \Delta L/\alpha_T$, respectively) in both advection and diffusion

258   dominated zones are less than 1, which is smaller than the upper limit of $P_e = 4$ to

259   effectively avoid numerical oscillations and instabilities.

260

261   **Table 1**. Parameters and values used in our numerical model simulations.

Parameters	Value	Description
Constant model parameters		
S_y	0.3	Specific yield [-]
λ	40	River boundary wave length [L]
α	5	River boundary amplitude [L]
θ	0.3	Efficient porosity [-]
J_x	0.0025	Base groundwater gradient [-]
σ	1.14	River boundary sinuosity [-]
t_d	10	Duration of flood event [T]
n_d	0.25	Skewness of flood event [-]
t_p	$n_d t_d$	Time to peak river stage [T]
H_0	1	Base river stage [L]
n_0	1	Intensity of flood event [-]
α_L	2	Longitudinal dispersivity [L]
α_T	$0.1\alpha_L$	Transverse dispersivity [L]
Variable model parameters		
Γ_d	0.1 1 10 100	Dimensionless aquifer transmissivity [-]
δ	90 70 50 20 10	Bank slope angle [°]

262

263   Similar to Gomez-Velez et al. (2017), we evaluated the impact of bank slope by

264 comparing the net hyporheic exchange flux ($Q^*_{net,\ HZ}(t)$), area of HZ ($A^{**}(t)$),

265 penetration distance of the HZ ($d^{**}(t)$) and mean RTD ($\mu_r^*(\mathbf{x}, t)$) between vertical and

266 sloping river bank models. A detailed definition of these variables is provided in the SI

267 (section S5).

268

3. Results

3.1 Effect of bank slope on hyporheic exchange flow and HZ extent

3.1.1 Hyporheic exchange flow

The flow field (velocity magnitude and direction) and net HEF ($Q^*_{net, HZ}(t)$) changed dynamically during and after the simulated flood event. Fig. 3a – 3d show the progression of net HEF for different aquifer transmissivity (Γ_d) and bank slope angle (δ) conditions. Snapshots of the flow field and the boundary of the HZ area (isolines of $C(\mathbf{x}, t) = 0.5$ as concentration of a conservative solute) for different δ conditions at different times (pink dots in Fig. 3a) for $\Gamma_d = 1$ are shown in Fig. 4a - 4f.
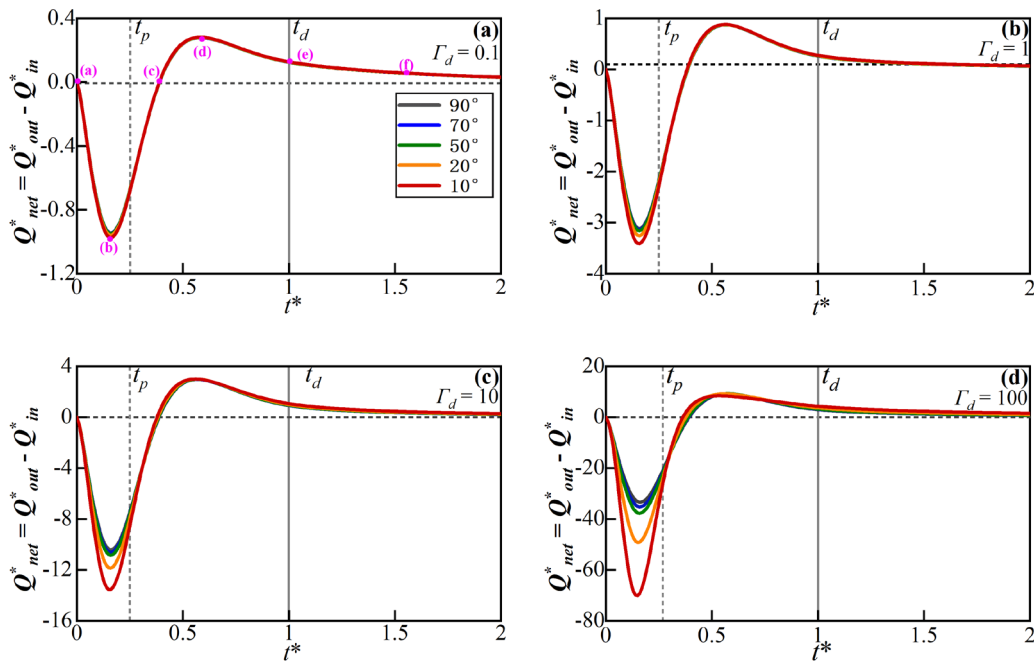
Figure 3. Temporal progression of dimensionless net HEF ($Q^*_{net, HZ}(t)$) for four different aquifer transmissivity values (represented by Γ_d) and bank slopes angles (δ, from 10-90 degrees). Time-to-peak flood (t_p) and flood duration (t_d) are marked by vertical dashed lines. Pink dots in (a) marked by (a) - (f) correspond to the snapshots of the flow field shown in Fig. 4. A negative flux value here represents water flow from

286 the river to the aquifer. Note that Γ_d negatively correlates with the transmissivity of the

287 aquifer.

288
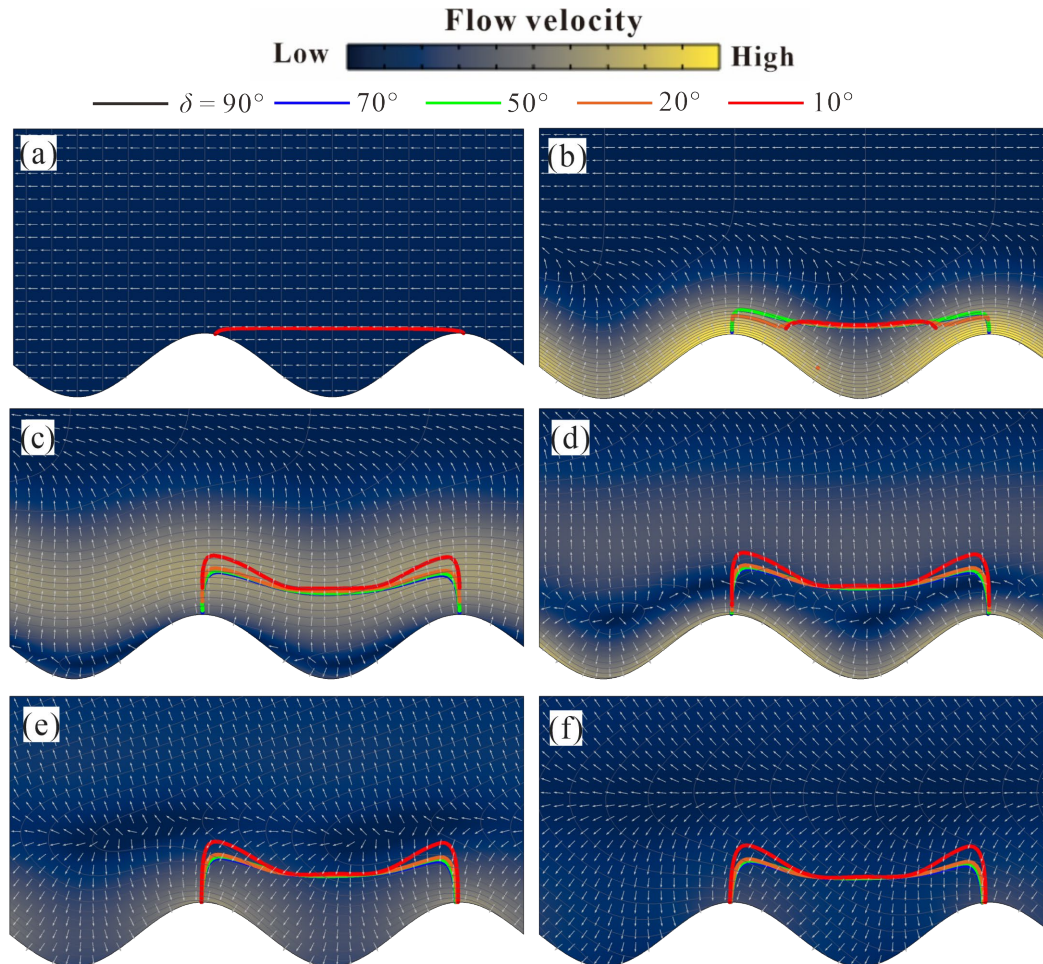
289

290 **Figure 4.** Plan view of the river channel and aquifer showing the temporal progression

291 of the alluvial flow field and spatial extent of the HZ. (a)-(e) are snapshots of the flow

292 field at different time steps ($t^* = 0, 0.16, 0.39, 0.57, 1, 1.5$) during the simulated event

293 (pink dots in Fig. 3a). Colored surfaces represent the magnitude of the Darcy flux vector

294 (blue is low and yellow is high) and white isolines the dimensionless hydraulic head.

295 Bold colored lines correspond to the HZ extent for different bank slope conditions.

296   Before the flood event ($t = 0$), steady-state base flow conditions are assumed, as

297 shown in Fig. 4a. The inflow and outflow (along the upstream and downstream meander

298 bend, respectively) are in balance. The bank slope has no effect on the HZ boundaries

299 before the flood event. Before peak river stage of the flood event is reached ($0 < t <$

300   0.25t_d), the onset of the flood event is indicated by the rising river stage and forces the

301   river to infiltrate into the aquifer along the SWI (negative values of $Q^*_{net, HZ}$ (t) in Fig.

302   3), resulting in the expansion of the HZ as shown in Fig. 4b. The influx of river water

303   into the HZ (-$Q^*_{net, HZ}$ (t)) reaches its maximum before the time-to-peak river stage (t =

304   0.25t_d) because the pressure wave propagates into the aquifer and decreases the head

305   gradient between the river and the connected aquifer. For higher transmissivity aquifers

306   (Lower Γ_d values in Fig. 3), bank slope has a reduced impact on net outflux as the fast

307   propagation of the pressure wave results in the hydraulic head near the SWI to be very

308   similar. Among different aquifer transmissivity conditions. As aquifer transmissivity

309   decreases, the ability of the aquifer to transmit the pressure wave becomes limited, and

310   the interaction flux is dominated by the location (displacement) of the SWI and the river

311   stage. On the other hand, a smaller slope angle induces a longer displacement of the

312   SWI (M(t)) away from the river, where the groundwater head adjacent to the SWI is

313   always relatively high (i.e., the head in base flow condition). This, consequently, leads

314   to a larger head gradient near the SWI as well as larger dimensionless net fluxes under

315   increasing Γ_d conditions as shown in Fig. 3.

316   The maximum dimensionless flux ratios $Q^*_{max, var} = Q^*_{max, s}$/ $Q^*_{max, v}$ of sloping (δ

317   < 90°, $Q^*_{max, s}$) vs vertical (δ = 90°, $Q^*_{max, v}$) riverbank cases are shown in Fig. 5, which

318   indicates the deviation in predicting peak net flux when neglecting the slope of the

319   riverbank. The bank slope is found to increase infiltration by up to 120% ($Q^*_{max, var}$ ≈

320   2.2) for Γ_d = 100 with δ = 10° while for larger slope angles or higher hydraulic

321   transmissivities the dimensionless infiltration gradually decreases.

322
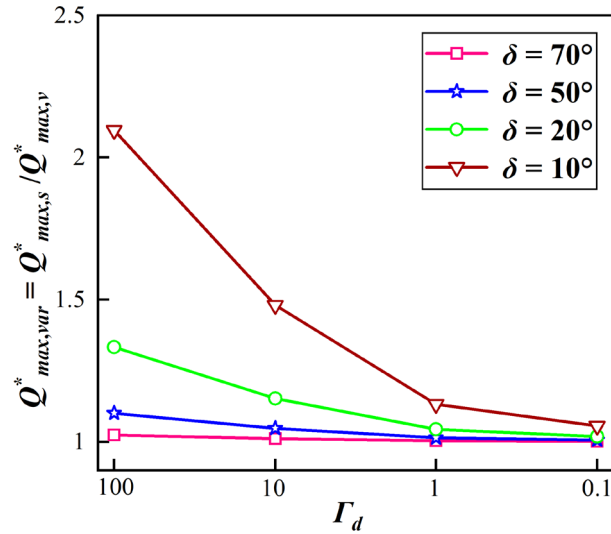
Figure 5. Ratio of maximum net flux for slope to no-slope (vertical river bank) conditions $Q^*_{max,var} = Q^*_{max,s}/Q^*_{max,v}$ for four aquifer transmissivities and slope angles. Note that Γ_d negatively correlates with aquifer transmissivity.

As the river stage decreases after t_p, the head gradient near the SWI gradually reverses and the net outflux starts increasing (the river is gaining water) as shown in Fig. 3. This is associated with the river stage declining below the groundwater level (see Fig. 4c - 4f). For the lowest hydraulic transmissivity condition ($\Gamma_d = 100$), bank slope can slightly extend the time required for the system to recover to initial conditions after t_p but in general, the response of the net outflux to bank slope is negligible when compared to that of the influx. Eventually, the net flux converges to zero, which indicates the flow field within the aquifer recovers to the initial conditions. The bank slope has no impact on the HEF after the duration of the flood event.

3.1.2 Patterns of hyporheic area and penetration distance

Fig. 6 and Fig. 7 show the temporal progression of the dimensionless HZ area ($A^{**}(t)$) and penetration distance ($d^{**}(t)$) into the alluvial valley relative to the initial condition for varying aquifer transmissivity (Γ_d) and slope angles.

342

343
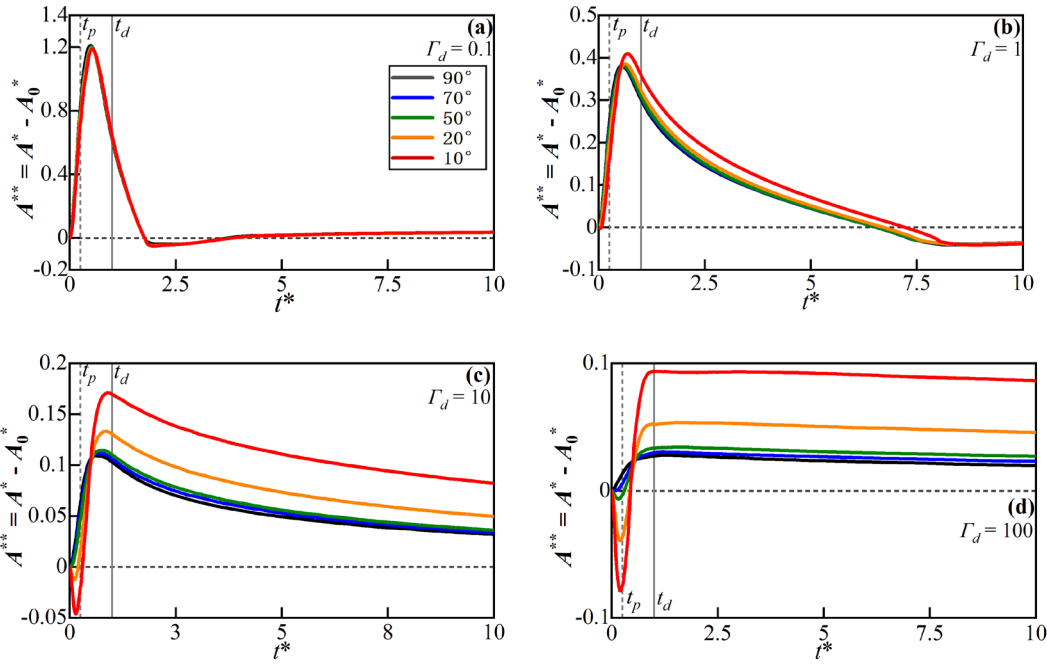
Figure 6. Temporal progression of dimensionless HZ area for different values of Γ_d and δ (colored lines). Time-to-peak (t_p) and flood duration (t_d) are marked by vertical dashed lines.

348

349
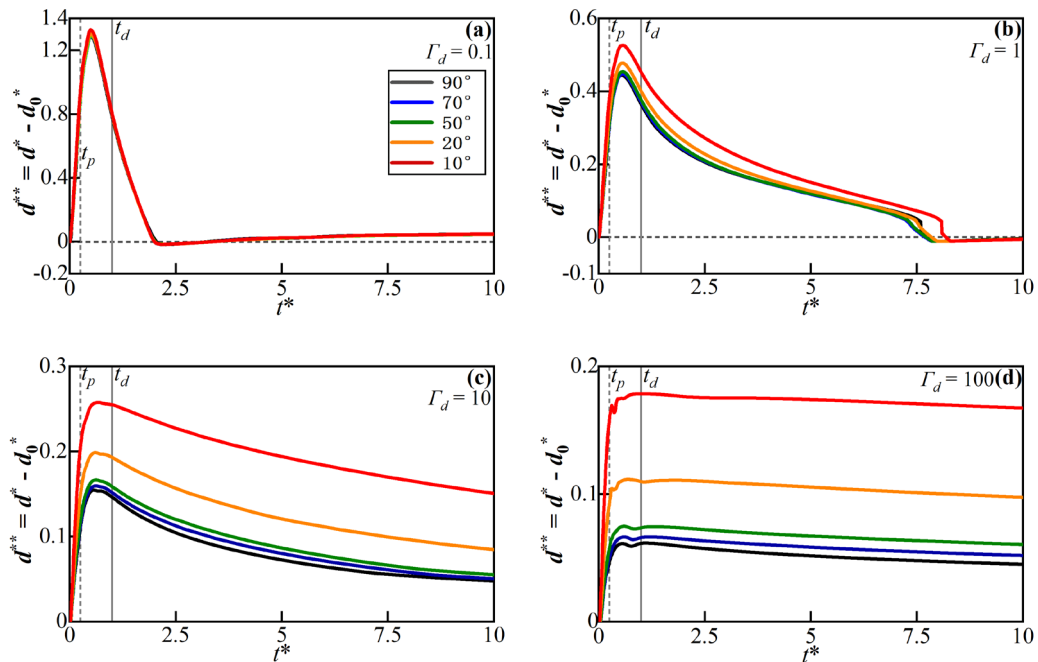
Figure 7. Temporal progression of dimensionless HZ penetration distance into the alluvial valley (d^{**}) for different values of Γ_d and δ (color lines). Time-to-peak (t_p) and flood duration (t_d) are marked by vertical dashed lines.

353   For vertical banks (δ = 90°, black lines in Fig. 6), the HZ area increases

354   synchronously with the river stage ($t < t_p$). After the peak time of the flood event ($t >$

355   t_p), the HZ area continues to extend as river water still recharges the aquifer. After the

356   flood event ($t > t_d$), the river water that was stored in the aquifer ($C(\mathbf{x}, t) > 0$) slowly

357   discharges back into the river channel. Thus, the HZ area and penetration distance

358   gradually rebound to initial conditions.

359   Under sloping riverbank conditions, the riverbank will at times be submerged by

360   the rising river stage. Fig. 6a and 7a show that the effects of bank slope on HZ area

361   ($A^{**}(t)$ in Fig. 6) and penetration distance ($d^{**}(t)$ in Fig. 7) are almost counteracted by

362   the high transmissivity of the aquifer while the influence of bank slope was negligible.

363   At the beginning of the flood event, Fig. 6b – 6d show that for conditions with smaller

364   sloping angle, HZ area can be less than zero (HZ at these times are smaller than the

365   initial condition). This is due to the fact that the movement of the SWI during a rising

366   river stage towards the alluvial valley will submerge parts that were previously

367   unsaturated as the aquifer with low transmissivity will propagate water more slowly.

368   As aquifer transmissivity decreases from Fig. 6b – 6d, the relative HZ area remains

369   negative for a longer time for smaller bank slopes. This indicates that bank slope has a

370   more pronounced effect on HZ extent in cases where aquifer transmissivity is large as

371   a low-transmissivity aquifer takes more time to propagate infiltrating river water.

372   After about half the flood duration ($t > 0.5t_d$), the HZ area (A^{**}) becomes positive

373   in all scenarios as the model domain previously submerged during the flood event re-

374   emerges. As aquifer transmissivity decreases (Fig. 6a – 6d and Fig. 7a – 7d), the impact

375   of bank slope gradually increases especially in low aquifer transmissivity conditions,

376   where smaller bank slope can increase the peak values of area and penetration distance,

377   and delay the arrival time-to-peak value of the relative HZ area. After the flood event

378   ($t > t_d$), the effect of bank slope is counteracted by the higher aquifer transmissivity and

379   only lower transmissivities have a significant impact on the HZ resulting in larger $A^{**}(t)$

380   and $d^{**}(t)$ as shown in Fig. 6b – 6d and Fig. 7b – 7d. For low transmissivity scenarios,

381   the bank slope can increase the peak area and penetration of the HZ by almost 200%.

382   **3.2 Spatiotemporal progression of mean residence time distribution**

383   The progression of spatiotemporal patterns of mean RTD (i.e., travel time of river

384   water in aquifer) is a useful evaluation method for identifying the dynamic variation of

385   aging and rejuvenation of hyporheic water. Here we use the mean RT ratio between a

386   sloping model and a vertical model $\mu_r^*(\mathbf{x}, t) = \log_{10}(\mu_{\tau\text{-}S}(\mathbf{x}, t)/\mu_{\tau\text{-}V}(\mathbf{x}, 0))$ to evaluate the

387   influence of bank slope on the prediction of mean RTD for a given location and time.

388   Fig. 8 presents mean RTDs for the initial condition, where $\mu_{\tau0\text{-}max}$ is the maximum RT

389   in the domain. It can be seen that the isolines representing the RT are almost horizontal

390   in the area extending from the river but RT near the upstream river bend is smaller than

391   downstream because the initial flow direction is towards the negative direction of the x

392   axis. Notably, $\mu(\mathbf{x}, 0)$ grows almost exponentially as y increases, and a positive

393   correlation to Γ_d at a given location is observed.

394

$$\log_{10}\mu_\tau(\mathbf{x},0)/\log_{10}\mu_{\tau\text{-}max}(\mathbf{x},0)$$
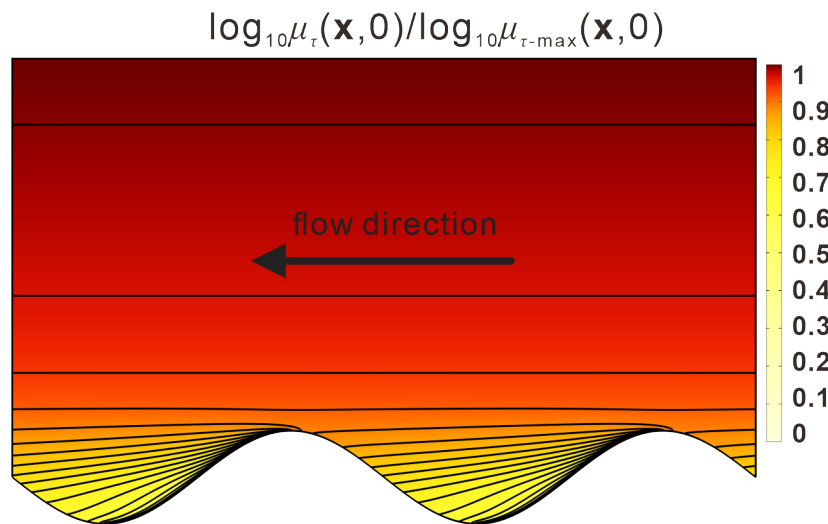
395

396   **Figure 8.** Plan view of relative mean residence time distributions [-] for baseline flow

397   conditions (no bank slope), which are represented by $\log_{10}\mu_\tau(\mathbf{x}, 0)/\log_{10}\mu_{\tau\text{-}max}(\mathbf{x}, 0)$ to

398   show the distribution pattern. The value of the contour lines grows exponentially with

399   the distance from the river meander.

400   Fig. 9 - 12 present five snapshots of μ_r^* for different bank slope angles and different

401   aquifer transmissivity values ($\Gamma_d = 0.1$, 1, 10 and 100, respectively). The five snapshots

402   represent the rising limb of the flood event ($t^* = 0.1$), the peak of the flood event ($t^* =$

403   0.25), the falling limb of the flood event ($t^* = 0.5$) and a time after the flood event (t^*

404   = 1, 2.5 and 10). The differences in residence time between sloping and vertical

405   riverbank models are within 12.2% in the white-colored areas ($-0.05 < \mu_r^* < 0.05$) of

406   Fig. 9 - 12, which indicates a minor effect of bank slope on mean RTD. The colored

407   areas in Fig. 9 – 12 indicate model results where neglecting bank slope will lead to an

408   overestimation ($\mu_r^* < -0.05$) or underestimation ($\mu_r^* > 0.05$) of residence (travel) times.

409
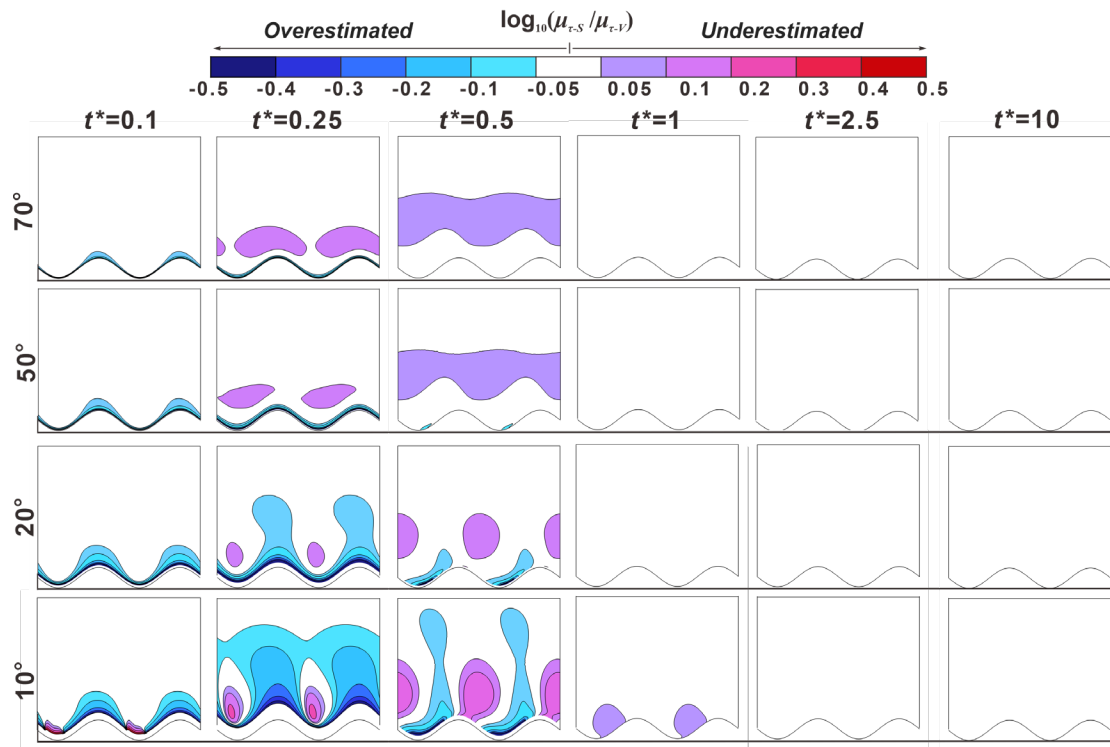
410

411   **Figure 9.** Five snapshots for the mean RTD ratio ($\mu_r^*(\mathbf{x}, t) = \mu_{r-S}^*(\mathbf{x}, t) / \mu_{r-V}^*(\mathbf{x}, t)$)

412   between sloping ($\mu_{r-S}^*(\mathbf{x}, t)$) and vertical riverbank conditions ($\mu_{r-V}^*(\mathbf{x}, t)$) at different

413   times t^* as a function of δ for $\Gamma_d = 0.1$. The horizontal lines beneath each figure are the

414   reference lines to show the initial location of the peak point of the point bar. The lower

415   sinuous lines at the reference lines are the initial SWIs. The colored areas indicate where

416   the bank slopes have significant impact on RT (difference in RT between sloping and

417   vertical model larger than 12.2%) and residence (travel) times of river water in the

418   aquifer would be overestimated (cold color area) or underestimated (warm color area)

419   if the effect of the bank slope was ignored.

420

421
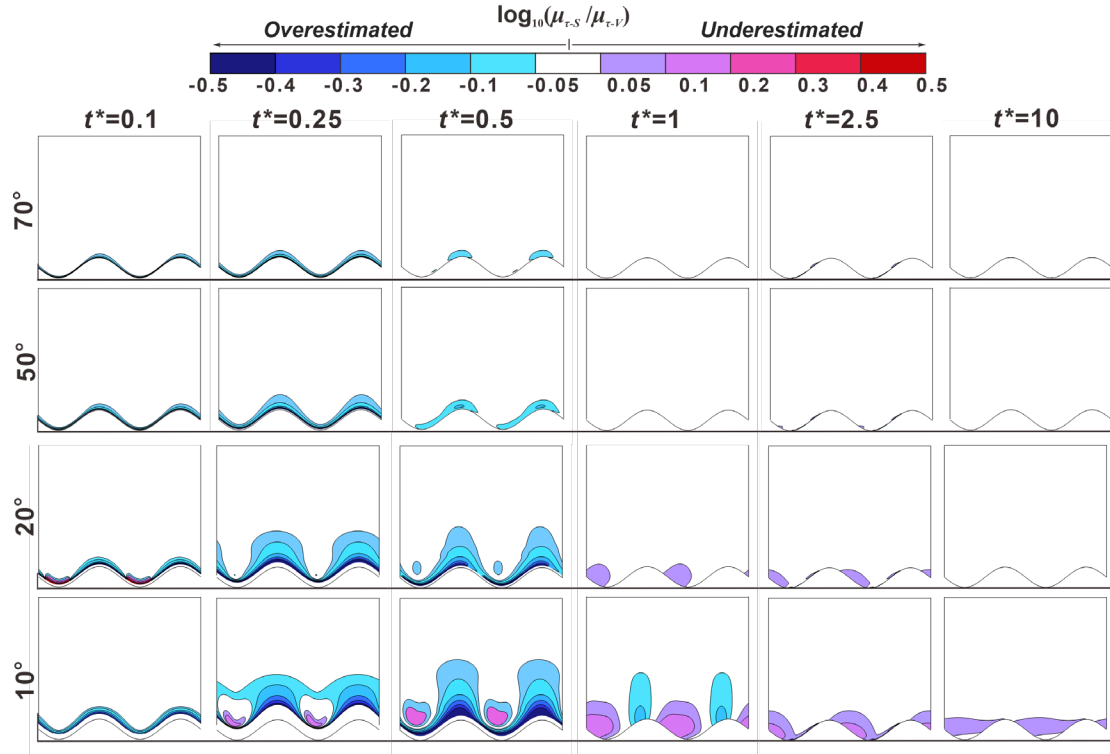
Figure 10. Five snapshots for the mean RTD ratio ($\mu_r^*(\mathbf{x}, t) = \mu_{r\text{-}S}^*(\mathbf{x}, t)/ \mu_{r\text{-}V}^*(\mathbf{x}, t)$) between sloping ($\mu_{r\text{-}S}^*(\mathbf{x}, t)$) and vertical riverbank conditions ($\mu_{r\text{-}V}^*(\mathbf{x}, t)$) at different times t^* as a function of δ for $\Gamma_d = 1$. The horizontal lines beneath each figure are the reference lines to show the initial location of the peak point of the point bar. The lower sinuous lines at the reference lines are the initial SWIs. The colored areas indicate where the bank slopes have significant impact on RT (difference in RT between sloping and vertical model larger than 12.2%) and residence (travel) times of river water in the aquifer would be overestimated (cold color area) or underestimated (warm color area) if the effect of the bank slope was ignored.

431

432
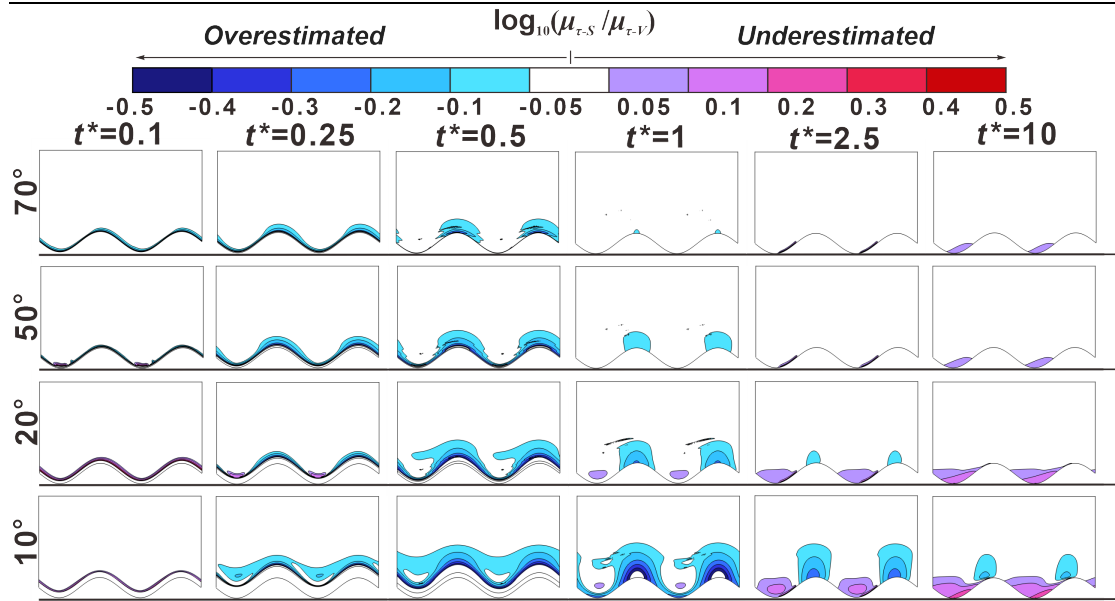
Figure 11. Five snapshots for the mean RTD ratio ($\mu_r^*(\mathbf{x}, t) = \mu_{r\text{-}S}^*(\mathbf{x}, t)/ \mu_{r\text{-}V}^*(\mathbf{x}, t)$) between sloping ($\mu_{r\text{-}S}^*(\mathbf{x}, t)$) and vertical riverbank conditions ($\mu_{r\text{-}V}^*(\mathbf{x}, t)$) at different times t^* as a function of δ for $\Gamma_d = 10$. The horizontal lines beneath each figure are the reference lines to show the initial location of the peak point of the point bar. The lower sinuous lines at the reference lines are the initial SWIs. The colored areas indicate where the bank slopes have significant impact on RT (difference in RT between sloping and vertical model larger than 12.2%) and residence (travel) times of river water in the aquifer would be overestimated (cold color area) or underestimated (warm color area) if the effect of the bank slope was ignored.

Figure 12. Five snapshots for the mean RTD ratio ($\mu_r^*(\mathbf{x}, t) = \mu_{r\text{-}S}^*(\mathbf{x}, t)/ \mu_{r\text{-}V}^*(\mathbf{x}, t)$) between sloping ($\mu_{r\text{-}S}^*(\mathbf{x}, t)$) and vertical riverbank conditions ($\mu_{r\text{-}V}^*(\mathbf{x}, t)$) at different times t^* as a function of δ for $\Gamma_d = 100$. The horizontal lines beneath each figure are the

448   reference lines to show the initial location of the peak point of the point bar. The lower

449   sinuous lines at the reference lines are the initial SWIs. The colored areas indicate where

450   the bank slopes have significant impact on RT (difference in RT between sloping and

451   vertical model larger than 12.2%) and residence (travel) times of river water in the

452   aquifer would be overestimated (cold color area) or underestimated (warm color area)

453   if the effect of the bank slope was ignored.

454   At $t^* = 0.1$, a smaller bank slope can lead to a shorter travel time of river water in

455   the aquifer (negative values of μ_r^*) near the SWI compared to the vertical riverbank

456   scenario. The area of shorter travel time caused by bank slope was positively related to

457   aquifer transmissivity. The effect of bank slope is small for $\Gamma_d = 10$ and 100 because the

458   groundwater mound (the raised groundwater stage) piles up around the river boundary,

459   but that small area extended deeper into the alluvial valley for smaller slope angles.

460   Due to the scattered and nested flow paths near the cut bank and point bar, respectively,

461   the area of the negative value of μ_r^* at the cut bank of the SWI is larger than that at the

462   point bar. The change of flow direction near the point bar leads to a prolonged flow path

463   for the water in the river channel as well as to forced groundwater mixing with the

464   slightly older water (Fig.8 shows that the water was potentially older in y direction

465   compared to $-x$ direction in the point bar). This effect was amplified with decreasing

466   bank slope angle, but it is only statistically significant ($\mu_r^* < -0.05$ or $\mu_r^* > 0.05$) when

467     $\delta = 10°$ at $t^* = 0.1$.

468   At the time of peak flood ($t^* = 0.25$), the river still infiltrates into the aquifer. For

469     $\Gamma_d = 0.1$, results of μ_r^* in Fig. 9 show that bank slope can lead to both overestimated and

470   underestimated RT areas. Both magnitude of relative RT (μ_r^*) and associated area

471   increase with decreasing slope due to the longer travel distance of river water into the

472   aquifer. As the slope angle decreases, the underestimated travel time area was located

473   closer to the peak of the cutbank. The impact of bank slope on mean RTD for $\Gamma_d = 1$

474   was rather similar in its pattern compared to $\Gamma_d = 0.1$, but the degree of that impact was

475   reduced. For $\Gamma_d = 10$ and 100, only overestimated travel time area can be seen near the

476   river bank with a smaller area of impact compared to smaller Γ_d conditions, because the

477   groundwater has not sufficiently propagated into the aquifer due to lower transmissivity.

478   At $t^* = 0.5$, part of the aquifer that was submerged at $t^* = 0.25$ reemerges due to

479   the decline in river stage. In most cases, smaller bank slopes can lead to wider

480   reemergence of the aquifer, which therefore results in overestimated travel time area

481   near the river boundary; however, this was not the case for $\Gamma_d = 0.1$ where bank slope

482   can both lead to overestimated and underestimated RT area. Furthermore, compared to

483   when $t^* = 0.25$, the impact of bank slope becomes weaker for $\Gamma_d = 0.1$, but more relevant

484   for the larger Γ_d values.

485   After the flood event ($t^* > 1$), the influence of bank slope on mean travel time is

486   nearly eliminated for $\Gamma_d = 0.1$ and 1 due to the high aquifer transmissivity. However,

487   for aquifers with lower transmissivity ($\Gamma_d = 10$ and 100), bank slope still has a

488   significant effect on RT at $t^* = 10$ and leads to underestimated and overestimated RT

489   areas near the point bar and the cut bank, respectively.

490   Overall, Fig. 9-12 indicate that the time when bank slope was relevant in predicting

491   RT (travel time of groundwater in aquifer) was determined by the transmissivity of the

492   aquifer. For more transmissive aquifers, the impact of bank slope on the prediction of

493   groundwater travel time cannot be neglected during the flood event ($0 < t < t_d$), but that

494   impact will be eliminated after the flood event due to the quick recovery of the aquifer

495   to baseline conditions. For lower transmissivity aquifers, bank slope plays an important

496   role on groundwater travel time after $t > 0.5^* t_d$ and has a more lasting influence on

497   aquifer RT, as more time is required to recover to initial conditions.

498   **3.3 Relative flux-weighted residence time**

499   Fig. 13 shows the progression of the flux-weighted relative RT $\mu^*_{out}(x, t) = \mathbf{n} \cdot Q^*_{out}(x,$

500      $t) \log_{10}(\mu_\tau(x, t)/\mu_\tau(x, 0))$ for different slopes and aquifer transmissivities. $M^*_{out}(x, t)$

501   represents the difference in flux-weighted RT of the water discharged into the river

502   compared to the initial condition. At the start of the flood event, there is no μ^*_{out} as river

503   water infiltrates the aquifer. Following the decline in river stage, the aquifer begins to

504   discharge the mixed water with different RT back into the river (see Fig. 4c).

505
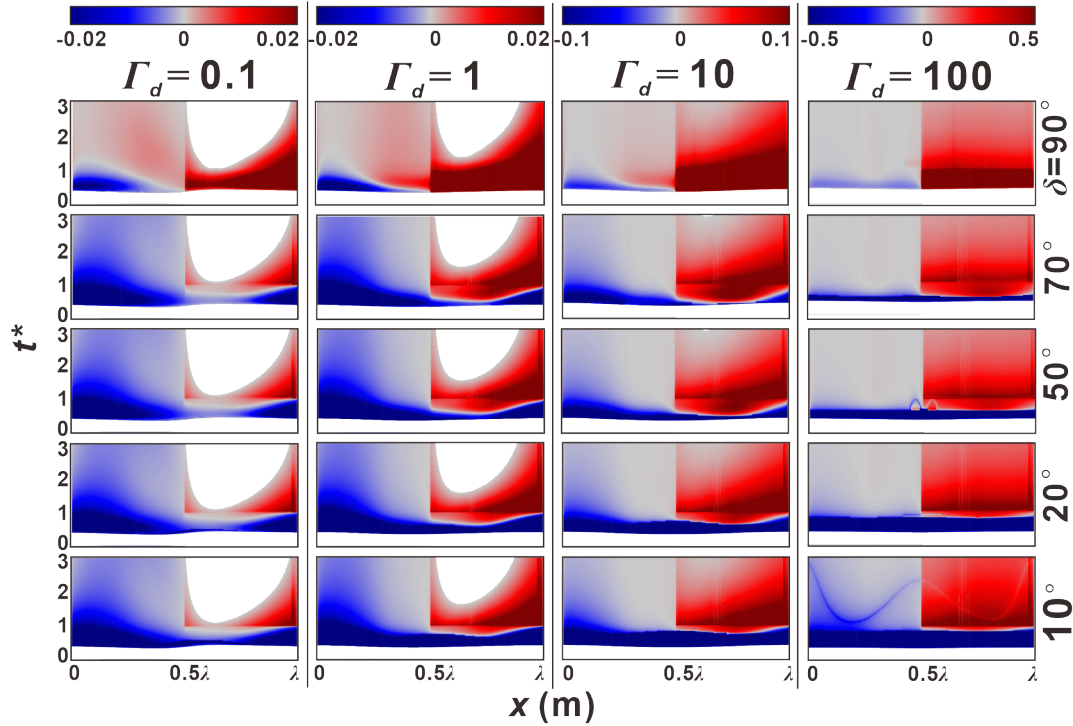
506

507   **Figure 13.** Temporal progression of flux-weighted ratios of RT to the RT for baseline

508   conditions ($\mu^*_{out}(x, t) = \mathbf{n} \cdot Q^*_{out}(x, t)\log_{10}(\mu_\tau(x, t)/\mu_\tau(x, 0))$) along the river meander as a

509   function of δ and Γ_d. $\mu^*_{out}(x, t)$ indicates the difference of flux weighted water RT (travel

510   time) that the aquifer discharges into river compared to the initial condition.

511   For vertical riverbank conditions ($\delta = 90°$, top row in Fig. 13), upstream ($0.5\lambda <$

512   $x < \lambda$) and downstream ($0 < x < 0.5\lambda$) boundaries of the meander bend discharge older

513   and younger water, respectively. The rejuvenated or aged waters that represent shorter

514   and longer travel times compared to the baseline condition, respectively, were mostly

515   discharged before the flood event ($t^* < 1$) due to the greater outflux as shown in Fig.

516   3a. It can also be seen that water was aged along the upstream bend compared to the

517   more rejuvenated water along the downstream bend. After the flood event, μ^*_{out}

518   gradually disappears along the upstream meander (blank areas) for $\Gamma_d = 0.1$ and 1,

519   because the flow fields were recovering to baseline conditions. Therefore, the upstream

520   meander gradually becomes the inflow boundary.

521   For cases with lower values of Γ_d (left columns in Fig. 13), μ^*_{out} reaches equilibrium

522   earlier compared to cases with higher Γ_d as an increasing bank slope angle causes μ^*_{out}

523   to gradually decrease the travel time of the outflowing water during the flood event.

524   For larger Γ_d, μ^*_{out} was totally dominated by rejuvenated water during the flood event.

525   Furthermore, smaller bank slope angles can both extend the time that younger water is

526   discharging along the downstream meander, and increase the difference in residence

527   times of these younger waters between sloping and vertical conditions.

528   **4. Discussion**

529   **4.1 Why we should account for bank slope**

530   Tilted riverbanks are common in nature and caused by erosion and bank collapse,

531   as has been observed at multiple scales (Zingg, 1940). Previous studies have shown that

532   bank erosion is stronger where the river planimetry is more sinuous, river stage varies

533   more frequently, or where the riverbank has larger sloping angles, ultimately leading to

534   a flatter bank (Zingg. 1940; Hagorty et al., 1995; Mayor et al., 2008; Puttock et al.,

535   2013). Yet, the impact of riverbank geometry and in particular bank slope on sinuosity-

536   driven lateral hyporheic exchange was ignored in most previous studies. Our results

537   clearly indicate that HZ characteristics (HEF, area and penetration distance of HZ into

538   the alluvial valley) can be underestimated along a meandering river depending on bank

539   slope conditions.

540   We show that not accounting for bank slope and river sinuosity can lead to an

541   underestimation of the infiltration rate of water from the river to the alluvial aquifer (by

542   up to 120%), as well as the area and penetration distance. This effect is more

543   pronounced for smaller bank slope angles (Fig 5), which can be more likely found in

544   lowland streams (Laubel et al., 2003), especially in areas with extensive cattle grazing

545   streamside (Trimble, 1994).

546   Doble et al. (2012), Siergieiev et al. (2015) and Liang et al. (2018), assessed the

547   influence of bank slope on HEF using a vertical cross-sectional profile. Siergieiev et al.

548   (2015) found that the impact of bank slope on HEF was proportional to the hydraulic

549   conductivity of the aquifer. However, we argue here that bank slope is more relevant in

550   rivers connected to aquifers with low hydraulic transmissivity (high hydraulic

551   conductivity or low specific yield). Furthermore, we show (Fig. 14 as example) that

552   using only one cross-sectional river profile perpendicular to the river axis does not

553   capture the effect of river sinuosity on HEF as bank storage decreases from point bar to

554   cut bank. This indicates that the accuracy of bank storage estimates can be improved

555   by including river sinuosity, which has often been omitted in the past. In a meandering

556   river with variable bank slope, river geometry thus has a sizable effect on bank storage

557   progression and HEF, and should be included in any scenarios.

558
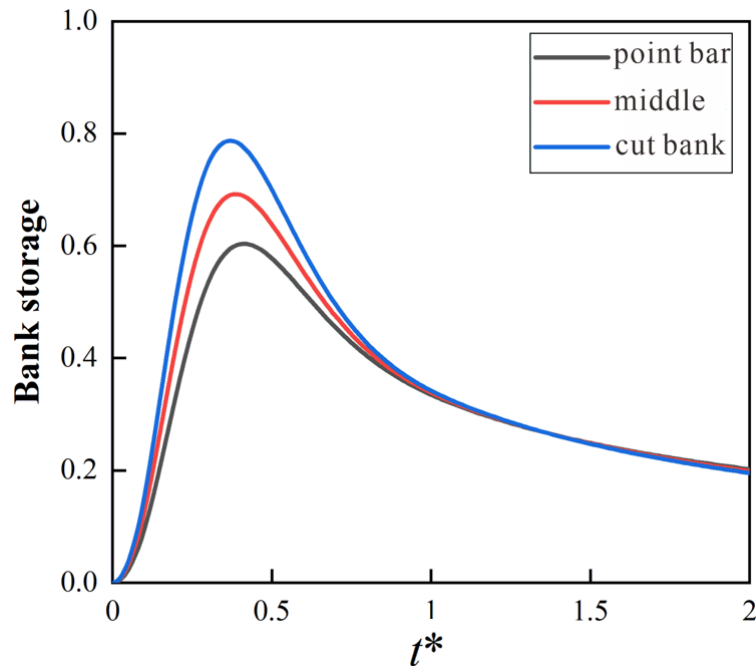
559

560   **Figure 14.** Bank storage versus time for $\Gamma_d = 1$ and $\delta = 90°$ condition at: the peak of

561   point bar ($x = 0$); middle ($x = 0.25\lambda$); peak of cut bank ($x = 0.25\lambda$). Dimensionless bank

562   storage was calculated by $\dfrac{\int_{Y(x,\,t)}^{Y(x,\,t)+4\lambda}[h\text{-}z_b\text{-}H_0]\mathrm{d}y}{\lambda H_p}$.

4.2 Implications of bank slope on biogeochemical reactions

Under rather stable flow conditions, hyporheic exchange rate and river sinuosity control the biogeochemical zonation (RTD) in the HZ. A higher hyporheic exchange rate (caused e.g., by a larger hydraulic conductivity in the aquifer or a more sinuous meander) will reduce the mean RTD promoting biogeochemical reactions (Boano et al., 2010; Gomez-Velez et al., 2012). However, for a transient flood event, the mean RTD could be both extended and reduced depending on the location with respect to the meander, due to variations in the complex flow paths (Gomez-Velez et al., 2017). Our results indicate that smaller bank slope angles could not only increase HEF and thus lead to increased transport of oxygen and nutrient rich stream water into the aquifer, but also alter the location and the residence time of this water within the aquifer system.

Mean RTDs of river water in the alluvial aquifer have been used to evaluate the potential for biogeochemical reactions by comparing the RT with biogeochemical timescales (BTS) for given solutes (Boano et al., 2010b; Gomez-Velez et al., 2012). Locations where the ratio of RT to BTS (expressed by Damköhler numbers) is small indicate a high reaction potential for that specific chemical species (Gomez-Velez t al., 2015; Pinay et al., 2015). It has been documented that the BTS for dissolved organic matter (DOC) can vary over ten orders of magnitude ($10^{-1} – 10^{9}$ d) (Hunter et al., 1998), while BTS for oxygen and nitrate have been found to vary over eight orders of magnitude ($10^{-2} – 10^{6}$ d) (Gomez-Velez et al., 2012). Here, we compare the mean RTD within the overlapping ranges of these two BTS for vertical and sloping riverbank conditions ($\delta = 10°$) at the peak time of the flood event ($t^{*} = 0.25$) for different aquifer transmissivity conditions, and show the zonation of residence times by using a BTS range of $10^{-1} – 10^{6}$ d (Fig. 15).
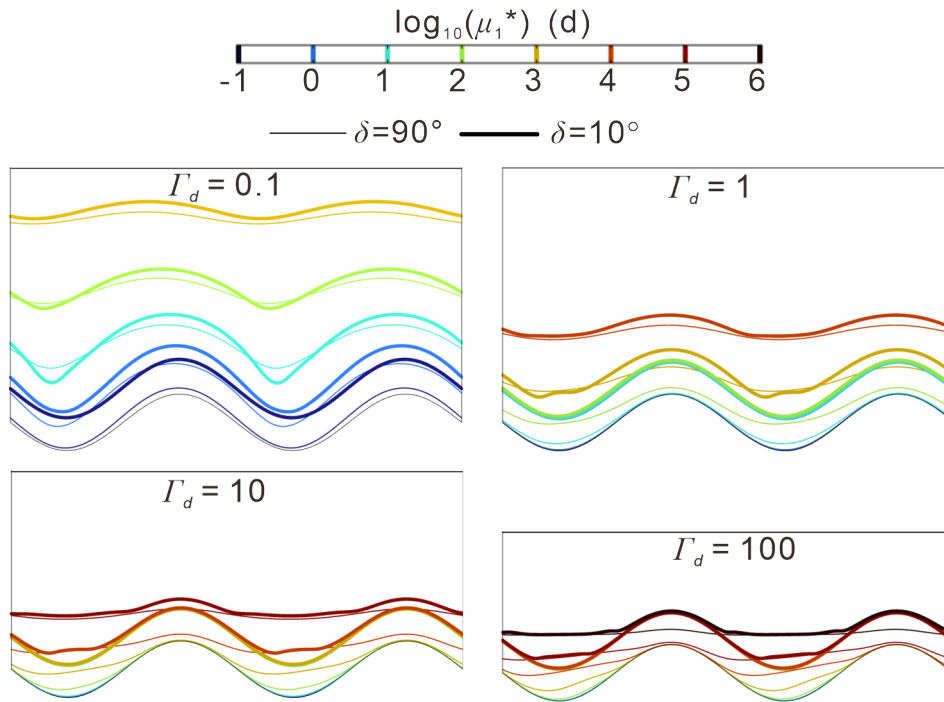
Figure 15. Plan view of the zonation of biogeochemical timescales (BTS, range of $10^{-1} - 10^6$) for common HZ constituents such as DOC, oxygen or nitrate for different aquifer transmissivities at $t^* = 0.25$. thick and thin lines indicate the comparison of vertical vs sloping riverbank ($\delta = 10°$) conditions, while the different colors indicate the different exponents. Unlike the previous mean RTD figures in which the relative mean RTD expressed in dimensionless form, the spatial scales of mean RTD in this figure are dimensional in days.

Fig. 15 indicates that neglecting bank slope impacts the prediction of reaction potentials during hyporheic exchange processes, especially for locations with short time scales. The reaction hot spots (areas indicated by the overlapping BTS ranges) for sloping riverbank conditions expanded further into the aquifer compared with the vertical bank conditions, similar to the overestimated areas in Fig. 9 to Fig. 12. Note that we did not aim to include specific reaction models in our study but instead used mean RTD as an indicator for various biogeochemical reactions in the aquifer. Furthermore, the wavelength of the river sinusoid in Fig. 15 was $\lambda = 40$ m to offer a representative riverbank-aquifer condition. The zonation of BTSs for larger and smaller river sinusoid wavelengths will be reduced towards the river boundary or further

606   expanded into aquifer, respectively, for both sloping and vertical riverbank conditions.

607   Although the dimensional BTS for various spatial scales are not shown here, similar

608   patterns between Fig. 9-12 and Fig. 15 imply the usability of the mean RTD results (Fig.

609   9-12) to infer on potential biogeochemical reactions.

610   The impact of bank slope on RT is basically controlled by aquifer transmissivity.

611   For higher aquifer transmissivity conditions, the impact of bank slope appears to be

612   more pronounced when the river stage rises during a flood event. For lower aquifer

613   transmissivity conditions, bank slope seems more relevant for mean RTD after the flood

614   event and its impact is more long-lasting. Smaller bank slope angles could extend (near

615   the point bar) or reduce (near the cut bank) pore water travel times throughout the flood

616   event, compared to the non-sloping (vertical) riverbank condition. This indicates that

617   compared with the vertical riverbank condition, point bars with bank slopes are more

618   favorable for removing dissolved organic carbon and for nitrification, while cut banks

619   with bank slope may have adverse effects on the groundwater quality near rivers. The

620   vertical profile modelling study of Derx et al. (2014) suggested for riverbank restoration

621   projects, increasing HEF by reducing the slope angle may have a negative effect on

622   restoration. The mean RTD results of this study also suggest that the impact of bank

623   slope on groundwater quality is determined by the location with respect to the meander

624   (near point bar or cut bank). As such, our analysis of mean RTDs can provide valuable

625   information on whether and where riverbank slope can induce biogeochemical hotspots

626   and hot moments and help guide choices to be made in biogeochemical field surveys

627   regarding location and sampling time under dynamic river stage conditions, especially

628   when the connected aquifers have low hydraulic transmissivity.

629

630   **4.3 Advantages and limitations of using a reduced 2-D model**

631   In this study, we propose a parsimonious reduced-order, idealized horizontal 2-D

632   model that simplifies the variation of the river-aquifer interface by using the moving

633   boundary method to depict the displacement of the SWI along a sloping riverbank. An

634   advantage of this approach is reduced model complexity as compared to a three-

635   dimensional model, which greatly reduces time and data requirements during model

636   building and computational demand during the simulation of HEF and especially

637   residence time distributions. Thus, our reduced-order model acts as a first step to gain

638   insight into the patterns of hyporheic exchange, riverbank storage and mean RTD in

639   settings with more complex riverbank morphology and dynamic forcing. Future efforts

640   should be focused on optimizing the computational method applied here and on

641   including more detailed morphology and hydrodynamic characteristics.

642   In our simulations we assume a constant bank slope angle along the entire

643   meandering river while natural riverbanks often change their slope angle from reach to

644   reach as well as with time. This variability could lead to more complex SWI travel

645   distances and residence time distributions, and new conceptualizations that account for

646   the contribution of bank slope on time-varying RTD and HZ extent are needed. In our

647   simulations we tested the model using a range of aquifer hydraulic conductivities.

648   Although hydraulic conductivity (or transmissivity) is a critical parameter in the

649   quantification of exchange fluxes and RTD between the two systems under varying

650   slope conditions, other parameters such as valley water head fluctuation, water

651   abstraction e.g. for agriculture or drinking water supply, peak flood event characteristics

652   or larger scale groundwater head fluctuation, e.g., due to changing groundwater

653   recharge in the context of changing rainfall patterns have not been considered here but

654   might also impact HZ extent, RTD and river-aquifer exchange flux. For example, valley

655   water head fluctuation and water abstraction in the aquifer will lead to a lower

656   groundwater table, increasing the hydraulic gradient between river and aquifer. This

657   will lead to the formation of a larger HZ area as well as longer travel distances and

658   times of river water in the aquifer. Thus, reducing the slope of the river bank could

659   reduce the infiltration of polluted river water into the riparian aquifer.

660   The current study assumes a perennial stream and unconfined (phreatic) conditions

661   in the connected aquifer as well as changing hydraulic gradients leading to gaining and

662   loosing conditions in the river. Where there is no hydraulic gradient between river and

663   aquifer, no large-scale infiltration of river water into the riverbanks will occur, while

664   local turbulent flow (e.g., due to obstacles in the river channel) might lead to localized

665   infiltration over short distances and short time scales (Sawyer et. al., 2011; Stonedahl

666   et al., 2013; Käser et al., 2013). Where the unconfined layer is small (e.g., in

667   mountainous headwater streams with a rather small sediment layer overlying a hard-

668   rock aquifer with relatively low hydraulic conductivity), the HZ is limited in its

669   maximum extent, and travel times and distances are considerably shorter. However, in

670   mountainous settings, slope angles are often much steeper due to erosion (here rivers

671   incising into the bedrock) and further simulations are required to better understand the

672   feedback between bank slope angle, hydraulic gradient and maximum extent of the

673   unconfined layer allowing for hyporheic exchange processes. These simulations will

674   also help us better understand the impact of bank slope on quantitative and qualitative

675   water supply to abstraction wells, e.g., used for the production of drinking water.

676   While using the Boussinesq equation neglects the influence of the vadose zone,

677   this approach as well as the assumption of a vertically integrated distribution of

678   hydraulic head have been widely used in the literature and proven adequate when

679   simulating sinuosity-driven HEF patterns (Boano et al., 2006; 2010., Cardenas. 2008;

680   2009a, b; Gomez-Velez et al., 2012; 2017, Kruegler et al., 2020). While we found

681   differences in HEF patterns when comparing simple models using the Boussinesq with

682   those using Richard's equation (S4 in SI) these differences exist independent of using

683   the DGM. However, we recommend in future studies to more systematically consider

684   these two different approaches with respect to their advantages and limitations, e.g., in

685   terms of computability or efficiency in predicting HEF under various conditions. While

686   in an ideal scenario a 3-D modeling approach includes vadose zone and riverbank slope

687   angle (both variable in time and space), for the moment the implementation of such

688   detailed models in practice suffers from limited computing capabilities.

5. Conclusions

689

690   The deformed geometry method was applied to characterize the expansion and
691 contraction of hyporheic zones along sloping riverbanks, and to evaluate the impact of
692 bank slope on hyporheic exchange flux, progression of the HZ area and residence
693 (travel) time distributions of the infiltrating water. To achieve this, several unconfined
694 alluvial aquifers with varying slope angles and aquifer transmissivity values were
695 simulated. Our results show that bank slope in a sinuosity-driven river was non-
696 negligible when the aims of numerical/analytical models are the prediction of the
697 progression of the hyporheic zone during and after a flood event (transient flood
698 forcing).

699   The overall findings of our work underline the need for including more realistic
700 riverbank morphological conditions into simulations when studying lateral hyporheic
701 exchange flow responses to dynamic forcings. Furthermore, our results show that more
702 detailed information on bank slope (e.g., through more measurements) can lead to a
703 better understanding of hyporheic flow patterns and potentially result in improved
704 biochemical process understanding for real-world conditions for more complex
705 morphological and depositional environments. Several conclusions can be drawn from
706 our study:

707 1. Sloping riverbanks can considerably increase HEF during a flood event, especially
708   when the river is connected to an alluvial aquifer with rather high hydraulic
709   conductivity and small bank slope angles as water can more easily infiltrate the
710   connected aquifer. Smaller bank slope angles can lead to an extended hyporheic
711   zone with river water infiltrating deeper (penetration distance) into the aquifer.
712   However, bank slope has only a minor impact on the hyporheic outflow flux (water
713   re-entering the stream).

714 2. During a flood event, the impact of bank slope on mean residence time distributions
715   (RTD) is more pronounced for aquifers with high hydraulic transmissivity, due to

716   the larger area and deeper penetration distance of the HZ for these conditions. On

717   the contrary, the impact of bank slope on mean RTD for lower transmissivity

718   aquifers is minor during the flood event, but bank slope can have a significant and

719   long-lasting effect post-flood.

720 3. River sinuosity should be considered when assessing the impact of bank slope on

721   mean RTD. Variable bank slope can lead to both longer and shorter residence times

722   when compared to vertical riverbank conditions.

723 4. Bank slope has a greater impact on the residence time of hyporheic water in lower-

724   transmissivity aquifers, thereby delaying the time of younger water discharge

725   downstream of a meander bend, which also delays the outflow of older water

726   upstream of that bend.

Code and data availability

Additional information regarding methodology and results is provided in the supporting information (SI).

Author contributions

YL: Conceptualization, Formal analysis, Methodology, Investigation, Writing

US: Conceptualization, Methodology, Writing

ZW: Funding acquisition, Software, Supervision

SK: Validation, Writing, Supervision

HL: Project administration, Supervision

Acknowledgements

This research was partially supported by the National Natural Science Foundation of China (Grant Numbers: 42272290, 41830862, and 42022018), and China Scholarship Council (CSC, 202106410042). Funding from the Royal Society (INF\R2\212060) for S.K. and the Leverhulme Trust (RPG-2021-030) for S.K. and U.S is also acknowledged.

Competing interests

The authors declare that they have no conflict of interest.

References

744 Bear, J., and Cheng, A. H. D.: Modeling groundwater flow and contaminant transport,
745   Vol. 23, pp. 83, Dordrecht: Springer, 2010.

746 Bertrand, G., Goldscheider, N., Gobat, J.-M., and Hunkeler, D.: Review: From multi-
747   scale conceptualization to a classification system for inland groundwater-
748   dependent ecosystems, Hydrogeology Journal, 20, 5-25, 2012.

749 Boano, F., Camporeale, C., Revelli, R., and Ridolfi, L.: Sinuosity-driven hyporheic
750   exchange in meandering rivers, Geophysical Research Letters, 33, L18406, 2006.

751 Boano, F., Harvey, J. W., Marion, A., and Packman, A. I., Revelli, R., Ridolfi, L., and
752   Wörman, A.: Hyporheic flow and transport processes: Mechanisms, models, and
753   biogeochemical implications, Reviews of Geophysics, 52, 603-679, 2014.

754 Boano, F., Demaria, A., Revelli, R., and Ridolfi, L.: Biogeochemical zonation due to
755   intrameander hyporheic flow, Water Resource. Research. 46, W02511, 2010.

756 Boano, F., Revelli, R., and Ridolfi, L.: Effect of streamflow stochasticity on bedform-
757   driven hyporheic exchange. Advances in Water Resources, 33(11), 1367-1374.
758   2010.Boulton, A. J., Datry, T., Kasahara, T., Mutz, M., and Stanford, J. A.: Ecology
759   and management of the hyporheic zone: Stream–groundwater interactions of
760   running waters and their floodplains, Journal of the North American Benthological
761   Society, 29 (1), 26-40, 2010.

762 Brunke, M., and Gonser, T.: The ecological significance of exchange processes between
763   rivers and groundwater, Freshwater Biology, 37 (1), 1-33, 1997.

764 Cardenas, M. B.: The effect of river bend morphology on flow and timescales of surface
765   water-groundwater exchange across pointbars, Journal of Hydrology, 362, 134-
766   141, 2008.

767 Cardenas, M. B.: A model for lateral hyporheic flow based on valley slope and channel
768   sinuosity, Water Resources Research, 45, W01501, 2009a.

769 Cardenas, M. B.: Stream-aquifer interactions and hyporheic exchange in gaining and

770   losing sinuous streams, Water Resources Research, 45, W06429, 2009b.

771   Cardenas, M. B.: Hyporheic zone hydrologic science: A historical account of its

772   emergence and a prospectus, Water Resources Research, 51, 3601-3616, 2015.

773   COMSOL Multiphysics. Introduction to COMSOL multiphysics. Version 5.5.

774   COMSOL. Burlington, MA. 2019.

775   Cooper, H. H., and Rorabaugh, M. I.: Ground-water movements and bank storage due

776   to flood stages in surface streams, Report of Geological Survey Water-Supply, pp.

777   1536-J, US Government Printing Office, Washington, United States, 1963.

778   Derx, J., Farnleitner, A. H., Blöschl, G., Vierheilig, J., and Blaschke, A. P.: Effects of

779   riverbank restoration on the removal of dissolved organic carbon by soil passage

780   during floods–A scenario analysis, Journal of Hydrology, 512, 195-205, 2014.

781   Doble, R. C., Crosbie, R. S., Smerdon, B. D., Peeters, L., and Cook, F. J.: Groundwater

782   recharge from overbank floods, Water Resources Research, 48 (9), W09522,

783   2012a.

784   Doble, R., Brunner, P., McCallum, J., and Cook, P. G.: An analysis of river bank slope

785   and unsaturated flow effects on bank storage, Ground Water, 50 (1), 77-86, 2012b.

786   Donea, J., A. Huerta, J.-P. Ponthot, and A. Rodriguez-Ferran.: Arbitrary Lagrangian–

787   Eulerian methods, In Encyclopedia of Computational Mechanics, ed. E. Stein, R.

788   de Borst, and T. J. R. Hughes, 413-434. New York: John Wiley & Sons, 2004.

789   Duarte, F., Gormaz, R., and Natesan, S.: Arbitrary Lagrangian–Eulerian method for

790   Navier–Stokes equations with moving boundaries, Computer Methods in Applied

791   Mechanics and Engineering, 193 (45-47), 4819-4836, 2004.

792   Fox, G. A., and Wilson, G. V.: The role of subsurface flow in hillslope and stream bank

793   erosion: a review, Soil Science Society of America Journal, 74 (3), 717-733, 2010.

794   Gao, Y., Zhu, B., Zhou, P., Tang, J. L., Wang, T., and Miao, C. Y.: Effects of vegetation

795   cover on phosphorus loss from a hillslope cropland of purple soil under simulated

796   rainfall: a case study in China, Nutrient Cycling in Agroecosystems, 85 (3), 263-

797   273, 2009.

798 Gomez-Velez, J. D., and Harvey, J. W.: A hydrogeomorphic river network model
799   predicts where and why hyporheic exchange is important in large basins,
800   Geophysical Research Letters, 41, 6403–6412, 2014.

801 Gomez-Velez, J. D., Wilson, J. L., and Cardenas, M. B.: Residence time distributions
802   in sinuosity-driven hyporheic zones and their biogeochemical effects, Water
803   Resources Research, 48 (9), 2012.

804 Gomez-Velez, J. D., Wilson, J. L., Cardenas, M. B., and Harvey, J. W.: Flow and
805   residence times of dynamic river bank storage and sinuosity-driven hyporheic
806   exchange, Water Resources Research, 53, 8572-8595, 2017.

807 Gomez-Velez, J. D., Harvey, J. W., Cardenas, M. B., and Kiel, B.: Denitrification in the
808   Mississippi River network controlled by flow through river bedforms, Nature
809   Geoscience, 8, 941-945, 2015.

810 Hagerty, D. J., Spoor, M. F., and Parola, A. C.: Near-bank impacts of river stage control,
811   Journal of Hydraulic Engineering, 121 (2), 196-207, 1995.

812 Hooke, J. M.: River meandering, In E. Wohl and J. Shroder (Eds.), Treatise on
813   geomorphology, Vol. 9, pp. 260-288, CA: Academic Press, San Diego, 2013.

814 Hester, E. T., and Gooseff, M. N.: Moving beyond the banks: Hyporheic restoration is
815   fundamental to restoring ecological services and functions of streams,
816   Environmental Science and Technology, 44 (5), 1521-1525, 2010.

817 Hunt, B.: An approximation for the bank storage effect, Water Resources Research, 26
818   (11), 2769–2775, 1990.

819 Hunter, K, S., Wang, Y., and Van, C, P.: Kinetic modeling of microbially-driven redox
820   chemistry of subsurface environments: coupling transport, microbial metabolism
821   and geochemistry. Journal of hydrology, 209 (1-4), 53-80, 1998.

822 Käser, D. H., Binley, A., and Heathwaite, A. L.: On the importance of considering
823   channel microforms in groundwater models of hyporheic exchange. River
824   Research and Applications, 29(4), 528-535, 2013.

825 Kiel, B. A., and Cardenas, M. B.: Lateral hyporheic exchange throughout the

826   Mississippi River network, Nature Geoscience, 7 (6), 413-417, 2014.

827 Krause, S., Abbott, B. W., Baranov, V., Bernal, S., Blaen, P., Datry, T., Drummond, J.,

828   Fleckenstein, J. H., Gomez-Velez, J., Hannah, D. M., Knapp, J. L. A., Kurz, M.,

829   Lewandowski, J., Marti, E., Mendoza-Lera C., Milner, A., Packman, A., Pinay, G.,

830   Ward, A. S., and Zarnetzke, J. P.: Organizational principles of hyporheic exchange

831   flow and biogeochemical cycling in river networks across scales, Water Resources

832   Research. 58, e2021WR029771, 2022.

833 Krause, S., Hannah, D. M., Fleckenstein, J. H., Heppell, C. M., Pickup, R., Pinay, G.,

834   Robertson, A. L., and Wood, P. J.: Inter-disciplinary perspectives on processes in

835   the hyporheic zone, Ecohydrology Journal. 4 (4), 481-499, 2011.

836 Krause, S., Lewandowski, J., Grimm, N., Hannah, D. M., Pinay, G., Turk, V., Argerich,

837   A., Sabater, F., Fleckenstein, J., Schmidt, C., Battin, T., Pfister, L., Martí, E.,

838   Sorolla, A., Larned, S., and Turk, V.: Ecohydrological interfaces as critical

839   hotspots for eocsystem functioning, Water Resources Research. 53, 6359-6376,

840   2017.

841 Krause, S., Tecklenburg, C., Munz, M., and Naden, E.: Streambed nitrogen cycling

842   beyond the hyporheic zone: Flow controls on horizontal patterns and depth

843   distribution of nitrate and dissolved oxygen in the upwelling groundwater of a

844   lowland river, Journal of Geophysical Research: Biogeosciences, 118 (1), 54-67,

845   2013.

846 Kruegler, J., Gomez-Velez, J. D., Lautz, L. K., and Endreny, T. A.: Dynamic

847   evapotranspiration alters hyporheic flow and residence times in the intrameander

848   zone, Water, 12 (2), 424, 2020.

849 Larkin, R. G., and Sharp, J. M.: On the relationship between river-basin geomorphology,

850   aquifer hydraulics, and groundwater flow direction in alluvial aquifers, Geological

851   Society of America Bulletin, 104, 1608-1620, 1992.

852 Laubel, A., Kronvang, B., Hald, A. B., and Jensen, C.: Hydromorphological and

853   biological factors influencing sediment and phosphorus loss via bank erosion in

854   small lowland rural streams in Denmark. Hydrological processes, 17(17), 3443-

855   3463, 2003.

856   Li, H., Boufadel, M. C., and Weaver, J. W.: Quantifying bank storage of variably

857   saturated aquifers, Ground Water, 46 (6), 841-850, 2008.

858   Liang, X. Y., Zhan, H. B., and Schilling, K.: Spatiotemporal responses of groundwater

859   flow and aquifer-river exchanges to flood events, Water Resources Research, 54

860   (3), 1513-1532, 2018.

861   Lindow, N., Fox, G. A., and Evans, R. O.: Seepage erosion in layered stream bank

862   material, Earth Surface Processes and Landforms, 34 (12), 1693-1701, 2009.

863   Mayor, Á. G., Bautista, S., Small, E. E., Dixon, M., and Bellot, J.: Measurement of the

864   connectivity of runoff source areas as determined by vegetation pattern and

865   topography: A tool for assessing potential water and soil losses in drylands, Water

866   Resources Research, 44 (10), 2008.

867   Maury, B.: Characteristics ALE method for the unsteady 3D Navier-Stokes equations

868   with a free surface, International Journal of Computational Fluid Dynamics, 6 (3),

869   175-188, 1996.

870   McCallum, J. L., Cook, P. G., Brunner, P., and D, Berhane.: Solute dynamics during

871   bank storage flows and implications for chemical baseflow separation, Water

872   Resources Research, 46: W07541, 2010.

873   McClain, M. E., Boyer, E. W., Dent, C. L., Gergel, S. E., Grimm, N. B., Groffman, P.

874   M., Hart, S. C., Harvey, J. W., Johnston, C. A., Mayorga, E., Mcdowell, W and

875   Pinay, G.: Biogeochemical hot spots and hot moments at the interface of terrestrial

876   and aquatic ecosystems, Ecosystems, 6 (4), 301-312, 2003.

877   Millar, R. G., and Quick, M. C.: Effect of bank stability on geometry of gravel rivers,

878   Journal of Hydraulic Engineering, 119 (12), 1343-1363, 1993.

879   Millington, R. J., and Quirk, J. P.: Permeability of porous solids, Transactions of the

880   Faraday Society, 57, 1200-1207, 1961.

881   Osman, A. M., and Thorne, C. R.: Riverbank stability analysis. I: Theory, Journal of

882   Hydraulic Engineering, 114 (2), 134-150, 1988.

883   Pinay, G., Peiffer, S., De Dreuzy, J. R., Krause, S., Hannah, D. M., Fleckenstein, J. H.,

884   Sebilo, M., Bishop, K., and Hubert-M, L.: Upscaling nitrogen removal capacity

885   from local hotspots to low stream orders' drainage basins, Ecosystems, 18 (6),

886   1101-1120, 2015.

887   Pohjoranta, A., and Tenno, R.: Implementing surfactant mass balance in 2D FEM–ALE

888   models, Engineering with Computers, 27 (2), 165-175, 2011.

889   Puttock, A., Macleod, C. J., Bol, R., Sessford, P., Dungait, J., and Brazier, R. E.:

890   Changes in ecosystem structure, function and hydrological connectivity control

891   water, soil and carbon losses in semi-arid grass to woody vegetation transitions,

892   Earth Surface Processes and Landforms, 38 (13), 1602-1611, 2013.

893   Seminara, G.: Meanders, Journal of Fluid Mechanics, 554, 271-297, 2006.

894   Schmadel, N. M., A. S. Ward, C. S. Lowry, and J, M. Malzone.: Hyporheic exchange

895   controlled by dynamic hydrologic boundary conditions, Geophysical Research

896   Letters, 43, 4408-4417, 2016.

897   Sawyer, A. H., Bayani Cardenas, M., and Buttles, J.: Hyporheic exchange due to

898   channel-spanning logs. Water Resources Research, 47(8), 2011.

899   Sharp, J. M.: Limitations of bank-stopage model assumptions, Journal of Hydrology,

900   35 (1-2), 31-47, 1977.

901   Siergieiev, D., Ehlert, L., Reimann, T., Lundberg, A., and Liedl, R.: Modelling

902   hyporheic processes for regulated rivers under transient hydrological and

903   hydrogeological conditions, Hydrology and Earth System Sciences, 19 (1), 329-

904   340, 2015.

905   Singh, T., Gomez‑Velez, J. D., Wu, L., Wörman, A., Hannah, D. M., and Krause, S.:

906   Effects of successive peak flow events on hyporheic exchange and residence times,

907   Water Resources Research, 56 (8), e2020WR027113, 2020.

908   Singh, T., Wu, L., Gomez-Velez, J. D., Lewandowski, J., Hannah, D. M., and Krause,

909   S.: Dynamic hyporheic zones: Exploring the role of peak flow events on bedform-

910   induced hyporheic exchange, Water Resources Research, 55, 218-235, 2019.

911   Stonedahl, S. H., Harvey, J. W., and Packman, A. I.: Interactions between hyporheic

912   flow produced by stream meanders, bars, and dunes, Water Resources Research,

913   49, 5450-5461, 2013.

914   Trimble, S. W.: Erosional effects of cattle on streambanks in Tennessee, USA. Earth

915   surface processes and landforms, 19(5), 451-464, 1994.

916   Triska, F. J., Kennedy, V. C., Avanzino, R. J., Zellweger, G. W., and Bencala, K. E.:

917   Retention and transport of nutrients in a third‐order stream in northwestern

918   California: Hyporheic processes, Ecology, 70 (6), 1893-1905, 1989.

919   Van Genuchten, M. T.: A closed‐form equation for predicting the hydraulic

920   conductivity of unsaturated soils. Soil science society of America journal, 44(5),

921   892-898, 1980.

922   Weatherill, J. J., Atashgahi, S., Schneidewind, U., Krause, S., Ullah, S., Cassidy, N.,

923   and Rivett, M. O.: Natural attenuation of chlorinated ethenes in hyporheic zones:

924   A review of key biogeochemical processes and in-situ transformation potential,

925   Water research, 128, 362-382, 2018.

926   Wondzell, S. M., and Swanson, F. J.: Floods, channel change, and the hyporheic zone,

927   Water Resources Research, 35 (2), 555-567, 1999.

928   Wu, L., Gomez‐Velez, J. D., Krause, S., Singh, T., Wörman, A., and Lewandowski, J.:

929   Impact of flow alteration and temperature variability on hyporheic exchange,

930   Water Resources Research, 56 (3), e2019WR026225, 2020.

931   Wu, L., Gomez-Velez, J. D., Krause, S., Wörman, A., Singh, T., Nützmann, G., and

932   Lewandowski, J.: How daily groundwater table drawdown affects the diel rhythm

933   of hyporheic exchange, Hydrology and Earth System Sciences, 25 (4), 1905-1921,

934   2021.

935   Wu, L., Singh, T., Gomez‐Velez, J. D., Nützmann, G., Wörman, A., Krause, S., and

936   Lewandowski, J.: Impact of dynamically changing discharge on hyporheic

937   exchange processes under gaining and losing groundwater conditions, Water

938   Resources Research, 54 (12), 10-076, 2018.

939   Zarnetske, J. P., Haggerty, R., Wondzell, S. M., and Baker, M. A.: Dynamics of nitrate

940   production and removal as a function of residence time in the hyporheic zone,

941   Journal of Geophysical Research, 116, G01025, 2021.

942   Zarnetske, J. P., Haggerty, R., Wondzell, S. M., Bokil, V. A., and González-Pinzón, R.:

943   Coupled transport and reaction kinetics control the nitrate source-sink function of

944   hyporheic zones, Water Resources Research, 48, W11508, 2012.

945   Zingg, A. W.: Degree and length of land slope as it affects soil loss in run-off,

946   Agricultural Engineering, 21, 59-64, 1940.

947